The Pennsylvania State University

The Graduate School

Department of Mechanical and Nuclear Engineering

DEVELOPMENT AND APPLICATION OF A REAXFF REACTIVE FORCE FIELD FOR HYDROGEN COMBUSTION

A Thesis in

Mechanical Engineering

by

Satyam Agrawalla

Submitted in Partial Fulfillment
of the Requirements
for the Degree of

Master of Science

August 2010

The thesis of Satyam Agrawalla was reviewed and approved* by the following:

Adri van Duin
Associate Professor of Mechanical Engineering
Thesis Advisor

Richard Yetter
Professor of Mechanical Engineering

Karen A. Thole
Professor of Mechanical Engineering
Head of the Department of Mechanical and Nuclear Engineering

*Signatures are on file in the Graduate School

ABSTRACT

To investigate the reaction kinetics of hydrogen combustion at high pressure and high temperature conditions, we constructed a ReaxFF training set to include reaction energies and transition states relevant to hydrogen combustion and optimized the ReaxFF force field parameters against training data obtained from Quantum Mechanical calculations and experimental values. The optimized ReaxFF potential functions were used to run NVT-MD simulations for various H_2/O_2 mixtures. We observed that the hydroperoxyl(HO_2) radical plays a key role in the reaction kinetics at our input conditions ($T \geq 2750K$, $P > 400atm$). The reaction mechanism observed is in good agreement with predictions of existing kinetic models for hydrogen combustion. Since ReaxFF derives its parameters from quantum mechanical data and can simulate reaction pathways without any preconditioning, we believe that atomistic simulations through ReaxFF could be a useful tool in enhancing existing kinetic models for prediction of hydrogen combustion kinetics at high pressure and high temperature conditions, which otherwise is difficult to attain through experiments.

TABLE OF CONTENTS

LIST OF FIGURES

LIST OF TABLES

ACKNOWLEDGEMENTS

My sincerest thanks to my advisor, Dr. Adri van Duin, for providing the opportunity to work on this project. I would also like to thank his research group members for constant help and support throughout the research.

Special thanks to the staff and Professors of Mechanical Engineering for being kind and supportive and making this experience worthy living it.

Finally, I wish to thank my family members and friends at Penn State for their constant motivation and support.

Chapter 1

INTRODUCTION

Hydrogen is one of the cleanest renewable energy sources. There are plentiful resources of hydrogen everywhere on this planet unlike fossil fuels. Its major advantages over other fuels is its high heat of combustion and zero CO_2 emission [1][2]. Due to increasing global warming, hydrogen is being considered as a possible replacement for fossil fuels. The prospect of a hydrogen based economy has increased interest in the use of hydrogen as a fuel and issues like storage and safety[3][4][5] are being resolved in order to use hydrogen as a fuel for practical purposes.

1.1 Problem Description

In order to extensively use hydrogen as a fuel, a detailed understanding of the chemical kinetics of hydrogen combustion is required. A good amount of understanding has already been achieved through extensive experiments and continuum-scale kinetic models in the past [6][7][8][9][10][11]. The reaction kinetics is well understood for low pressure and high temperature conditions and is dominated by chain branching reactions shown in reaction R1,R2 and R3.

$H+O_2 \rightarrow OH + O$ (R1)

$O + H_2 \rightarrow H + OH$ (R2)

$OH + H_2 \rightarrow H_2O + H$ (R3)

However, at very high pressure conditions (P > 400 atm), the reaction kinetics is still not well understood. Mueller et al[8] have suggested that the reaction kinetics in the zone above the extended second explosion limit* involves the formation and consumption reactions of HO_2 and H_2O_2 which are less understood as of now. Among the current kinetic models for H_2/O_2 combustion, Li et al[9] have validated their model with experimental data for a wide range of input conditions (298-3000K, 0.3-87 atm, Φ = 0.25-5.0) and found excellent agreement. Strohle et al[10] have evaluated several existing kinetic models of H_2/O_2 combustion under gas turbine conditions(pressure up to 33 atm)and concluded that O'Conaire Mechanism[11] and Li Mechanism[9] are most appropriate kinetic models for predicting reaction kinetics under these conditions . However, at very high pressures (P> 400 atm) it is difficult to obtain experimental data and none of the existing continuum-scale kinetic models have been validated for such elevated pressures.

This issue has prompted a shift to reaction kinetic modeling at an atomistic scale for high pressure conditions. Atomistic methods derived from solving the Schrodinger equation defined in Quantum Mechanics(QM) theory give an accurate prediction of reaction barriers and reaction energy for individual reactions. These methods do not require experimental validation. While these methods can be very useful to study reaction kinetics, they are computationally very expensive. They can be applied in dynamical simulations of a system of H_2/O_2 molecules but these simulations are limited to small systems and short time-scales [12]. This makes it difficult to use them for getting a detailed, statistically relevant description of the H_2/O_2 reaction

*Extended Second explosion limit: This is defined as a pressure-temperature boundary which indicates pressure, temperature points at which the rate of removal of H radicals occurs equally from reactions R1 pathway and R2 pathway.

$H + O_2 \rightarrow OH + O$ (R1) &

$H + O_2 + M \rightarrow HO_2 + M$ (R2)

R1 dominates in the region below this boundary can be classified as low-pressure zone and R2 dominates in the the region above and can be classified as high pressure zone. This will be explained in further detail in Chapter 2.

chemistry. Empirical methods, including tight-binding and force-field (FF) based approaches, provide a computationally inexpensive alternative to QM methods. While FF- methods are mainly used for non-reactive systems [13][14][15][16][17], currently a number of reactive FF-methods are available [18][19][20][21] that enable nanosecond-scale simulations of reactive systems of size >>1000 atoms. In our research we will present the development of an application of one such reactive force field called ReaxFF [22] for hydrogen combustion reactions. ReaxFF is a quantum derived FF which retains nearly the accuracy of results from QM for both reaction energies and transition states. It was developed in order to simulate the formation and dissociation of bonds correctly and does not require pre-defined reactive sites or reaction pathways to simulate a chemical reaction. Since the FF parameters are derived solely from QM data, ReaxFF can be directly applied to systems that cannot be studied experimentally. With increasing applications of high pressure combustion, like in rocket engines and shock induced reactions, ReaxFF could be a useful tool to enhance our understanding of the chemical kinetics of hydrogen combustion at high pressures.

1.2 Research Objectives

In this research work we will demonstrate the development of a ReaxFF FF to carry out molecular dynamics (MD) simulations for investigating the chemical kinetics involved in hydrogen combustion. We will present here the optimization of ReaxFF FF by training against QM derived transition states and reaction energy that are relevant to hydrogen oxidation. The ReaxFF FF will be applied on a system of H_2/O_2 molecules with various input conditions. The results will be analyzed to study the initiation reaction and reaction mechanism and estimate the overall activation energy of the water formation reaction. This research will demonstrate the

ability of ReaxFF as a computational method to describe the chemical events involved in hydrogen combustion process and should provide an accurate tool for analyzing the reaction mechanism under a wide range of input conditions.

1.3 Thesis Organization

The thesis is organized into a total of five chapters. The second chapter will give an introduction to the current knowledge of hydrogen combustion kinetics and the concepts of Molecular Dynamics, ReaxFF and Quantum Mechanics for simulating a reactive system of particles. The third chapter gives the methodology followed in this research work to develop the ReaxFF and demonstrate its validity. Chapter four will discuss the methodology followed to simulate hydrogen combustion and the input conditions used. It will also show the analysis of MD results to explain the reaction kinetics observed. Chapter five provides a conclusion of all the results and discusses possible future work.

Chapter 2

CONCEPTS OF HYDROGEN COMBUSTION AND MOLECULAR DYNAMICS

2.1 Hydrogen Combustion Kinetics

The current understanding of Hydrogen Combustion kinetics is best represented by the classical explosion limit diagram [6][23] shown in figure 2-1. The figure depicts explosion limits of stoichiometric mixtures of hydrogen and oxygen through pressure-temperature boundaries which separate regions of slow and fast reactions.

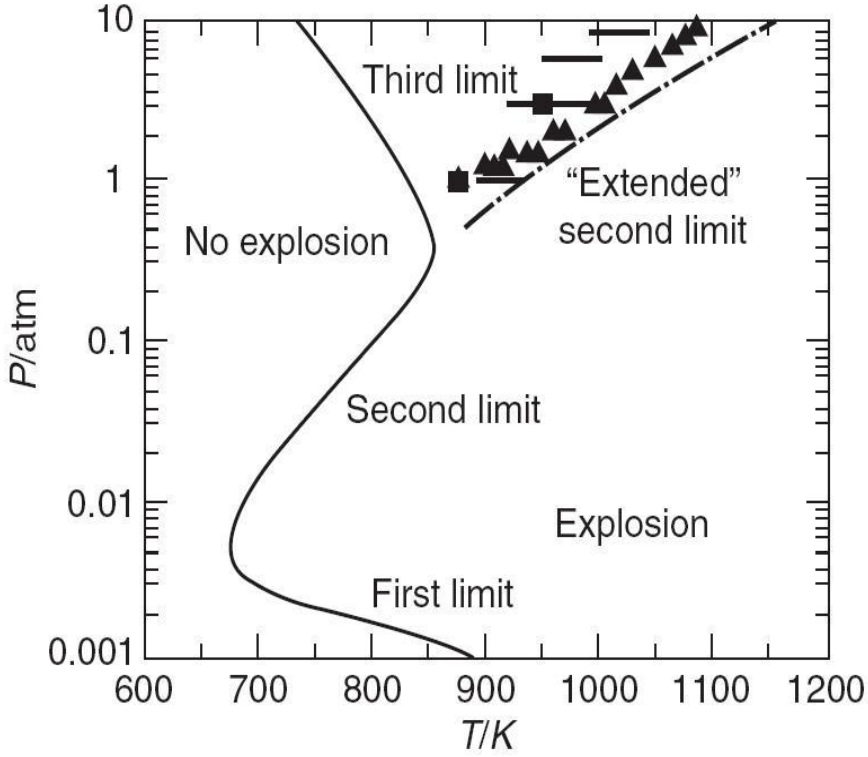

Figure **2-1**: Figure shows explosion limits of a stoichiometric H_2/O_2 mixture.

The initiation reaction of a H_2/O_2 mixture is given by

$H_2 + M \rightarrow 2H + M$ (R4)

Earlier studies [24] have also suggested other possible initiation reactions like

$H_2 + O_2 + M \rightarrow H_2O_2 + M$ (R5)

$H_2 + O_2 \rightarrow H + HO_2$ (R6)

These initiation reactions R4 and R6 essentially provide radicals which participates in chain propagating and chain branching reactions leading to the formation of a radical pool of H, O and OH radicals. These radicals react very quickly, creating more radicals in each reaction leading to an explosive condition.

The reaction mechanism in the zone between the first and second explosion limit in figure 2-1consists of a set of chain branching and chain propagation reactions as given below.

$H + O_2 \rightarrow O + OH$ (R7)

$H_2 + O \rightarrow H + OH$ (R8)

$H_2 + OH \rightarrow H_2O + H$ (R9)

The reactions R7 and R8 are chain branching, while R9 is chain propagating leading to water formation and H radical as chain carrier. The rate of the reactions R7, R8 and R9 increases with temperature and hence these reactions occur predominantly at high temperature conditions. However, as we increase the pressure of the mixture, there occurs a no explosion zone above the second explosion limit(as shown in figure 2-1). This is due to a competing reaction R10 which leads to formation of a relatively unreactive HO_2 radical.

$H + O_2 + M \rightarrow HO_2 + M$ (R10)

The reaction R10 is a pressure-dependent reaction and requires a third body collision(M) for reaction to occur. It competes directly with R7 and exceeds the rate of reaction R7 above the second explosion limit. The reaction R10 acts as a chain-terminating step due to formation of a meta-stable hydroperoxyl radical leading to no explosion zone. As we further increase the pressure into the third explosion limit, HO_2 radicals participate in a set of chain branching and propagating reactions given below, leading once more to explosive conditions.

$HO_2 + H_2 \rightarrow H_2O_2 + H$ (R11)

$HO_2 + HO_2 \rightarrow H_2O_2 + O_2$ (R12)

$H_2O_2 + M \rightarrow 2OH + M$ (R13)

$HO_2 + H \rightarrow 2OH$ (R14)

Hence HO_2 and H_2O_2 play a crucial role in reaction kinetics of H_2/O_2 mixtures at high pressure and low temperature conditions.

We observe that the reaction mechanism of H_2/O_2 mixtures revolves around H, O and OH radicals at low pressure and high temperatures (R7-R9) while HO_2/H_2O_2 reactions(R11-R14) become important at high pressure and low temperature conditions. This divide in reaction kinetics can be further emphasized by the extended second explosion limit (shown in figure 2-1) which depicts the pressure-temperature boundary for which the rate of reactions of R7 and R10 are same. This can be mathematically represented as

$$\frac{2k_7}{k_{10}} = [M] \quad (2.1)$$

using a steady state analysis, as can be seen in Glassman[24]. In equation (2.1) k_7 and k_{10} are the rate constant of reaction R7 and R10 respectively. $[M]$ represents the concentration of the third body M in reaction R10. Below the extended second explosion limit, we can expect to see more of H, O and OH chemistry while above it we can expect more of HO_2/H_2O_2 chemistry.

A list of all the important reactions in hydrogen combustion along with their heat of reactions and activation energy is compiled in Table 3-2 of chapter 3. The rate constants for each of this reaction can be found in Li et al[9].

2.2 Molecular Dynamics(MD)

MD is a simulation technique to calculate trajectory of a molecular system and evaluate its thermodynamic properties. It was first introduced by Alder and Wainwright in the late 1950's to study the interactions of hard spheres[25].

MD assumes that the classical Newton's equations of motion hold true at the molecular level. With proper choice of interaction potential between the particles, MD can predict very accurately the equilibrium properties of a system and can act as a potent replacement for experiments. MD simulations are now routinely used to investigate structure, dynamics and thermodynamics of a molecular system. Notable applications include the study of biological molecules and their complexes, especially protein structure determination and refinement[26]. MD is also used to study thin-film growth and ion sub-plantation[27].

2.2.1 Methodology:

Consider a system of N particles kept inside a cubic box of volume V. MD simulation consists of step by step solution of the Newton's equation of motion (2.2) and (2.3) for this system of particles for given initial position and velocities.

$$F_i = m_i \frac{dv_i}{dt} \tag{2.2}$$

$$v_i = \frac{dr_i}{dt} \tag{2.3}$$

In equation (2.2) and (2.3) , F_i is the force acting on the i^{th} particle of mass m_i, position r_i and velocity v_i. In the absence of external force, the total energy of the system is conserved. Hence, the force acting on every particle is conservative and can be expressed in terms of potential energy as

$$F_i = -\nabla U(r_i) \tag{2.4}$$

$$U(r_i) = u(r_i) + \sum_{j,i<j} u(r_i, r_j) + \sum_{j,i<j} \sum_{k,j<k} u(r_i, r_j, r_k) + \cdots \quad (2.5)$$

where $U(r_i)$ is the potential energy of the system at the point r_i, describing the interaction between particles of the system and the effect of external forces. Equation 2.5 represents $U(r_i)$ as the sum of external potential field $u(r_i)$, pair potential field $u(r_i, r_j)$ and many body potential fields like three-body interaction potential $u(r_i, r_j, r_k)$,four-body interaction potential $u(r_i, r_j, r_k, r_l)$ and so on. In practice only a few of the potential terms are kept, to the extent that these approximations are accurate.

Since, one can calculate the acceleration, velocity and position of the particle at any instant of time using equation 2.2 and 2.3, MD is a deterministic method. However, in order to be able to use MD as a replacement for real experiments, the trajectory information from a MD simulation needs to be converted to macroscopic thermodynamic properties, obtainable through real experiments. Using the ensemble theory of statistical thermodynamics, the trajectory information can be used to evaluate properties of the system like temperature, pressure, heat capacity etc.

2.2.2 Ensemble Theory:

Ensemble theory was first introduced by the American scientist J. Willard Gibbs[28]. An ensemble is defined as a collection of very large number of systems, each of which has identical macroscopic thermodynamic properties. The ensemble theory is used to obtain the particle distribution at thermodynamic equilibrium, using which other macroscopic thermodynamic properties are derived. The ensemble theory is based on the ergodic hypothesis as explained in the next section(2.2.2.1).

2.2.2.1 Ergodic Hypothesis:

The ergodic hypothesis states that the time average of a system thermodynamic variable is equal to its ensemble average i.e. the average of instantaneous value of this thermodynamic variable in each member of the ensemble. This hypothesis can be justified through the example of a roulette wheel. Consider the probability of spinning a number 5 on the roulette wheel. It can be either found by spinning the roulette wheel N number of times and calculating the number of times 5 occurs, or it can be calculated by spinning N identical roulette wheels at a time and seeing how many roulette wheels give 5 as the output(N is a very large number). This hypothesis holds true when the spins are mutually exclusive. While the first method is similar to time averaging, the latter method corresponds to ensemble averaging.

Using the ensemble theory, a molecular partition function is derived which indicates how the particles in a thermodynamic system are partitioned among the various available energy levels. Using this partition function one can directly calculate macroscopic thermodynamic properties.

Several types of ensembles have been formulated to replicate real experiments and the most commonly used ensembles have been explained in the following sections.

2.2.2.2 Microcanonical Ensemble:

This is composed of large number of isolated systems of particles, each of which has same number of particles (N), same volume(V) and same internal energy(U). Such an ensemble is easy to simulate, since the total energy of an isolated system i.e. the internal energy is inherently conserved in an MD simulation.

2.2.2.3 Canonical Ensemble:

This ensemble is composed of large number of closed isothermal systems of particles, each of which has same number of particles (N), same volume(V) and same temperature(T). In order to simulate a system of particles belonging to this type of ensemble, one needs to use a thermostat which can keep the temperature of the system fixed. In such a system, the internal energy is not necessarily conserved. One commonly used thermostat for the canonical ensemble is the Berendsen thermostat[29]. The Berendsen thermostat maintains a constant temperature by virtually coupling the system to an external heat bath which is fixed at the desired temperature. This is achieved by rescaling the velocities of the particles of the system such that

$$\frac{dT}{dt} = \frac{1}{\tau}(T_{bath} - T(t)) \tag{2.6}$$

where T_{bath} is the desired temperature and $T(t)$ is the system temperature and τ is a coupling constant whose magnitude determines how tightly the bath and system are coupled. A smaller value of τ implies a stronger coupling and vice-versa. Some other commonly used thermostats are Anderson thermostat[30] and Nose'-Hoover thermostat[31][32][33].

2.2.2.4 Grand Canonical Ensemble:

This ensemble is composed of large number of open, isothermal systems of particles, each of which has same chemical potential (μ), same volume(V) and same temperature(T). In this case the number of particles(N) in a system may not necessarily be constant. This ensemble is useful for adsorption studies; it was not used in the work presented in this thesis.

2.2.2.5 Isothermal-Isobaric Ensemble:

This ensemble is composed of large number of closed, isothermal and isobaric systems of particles, each of which has same number of particles (N), same pressure(P) and same temperature(T). This ensemble represents systems which are similar to macroscopic systems used in real experiments. The temperature is kept constant using a thermostat, while the pressure is kept constant using a barostat like Anderson barostat[30] and Rahman-Parinello barostat[34]. The barostat works by rescaling the volume of the system at each time step, to maintain constant pressure.

In the 'dilute limit'[28], the average equilibrium particle distribution is found to converge to the Maxwell-Boltzmann distribution, which covers most cases of practical applications.

2.2.2.6 Maxwell-Boltzmann distribution:

Maxwell-Boltzmann distribution represents the equilibrium particle distribution for an isolated system of independent particles at a given temperature. This best represents a monoatomic ideal gas and the speed distribution is given as

$$f(V) = \frac{m}{k_b T} V exp(-\frac{1}{2k_b T} m V^2) \tag{2.7}$$

where m is the mass of the particle, V is the speed of the particle and k_b is the Boltzmann's constant. This distribution is represented in figure 2-2 where V_{mp} represents the most probable particle speed.

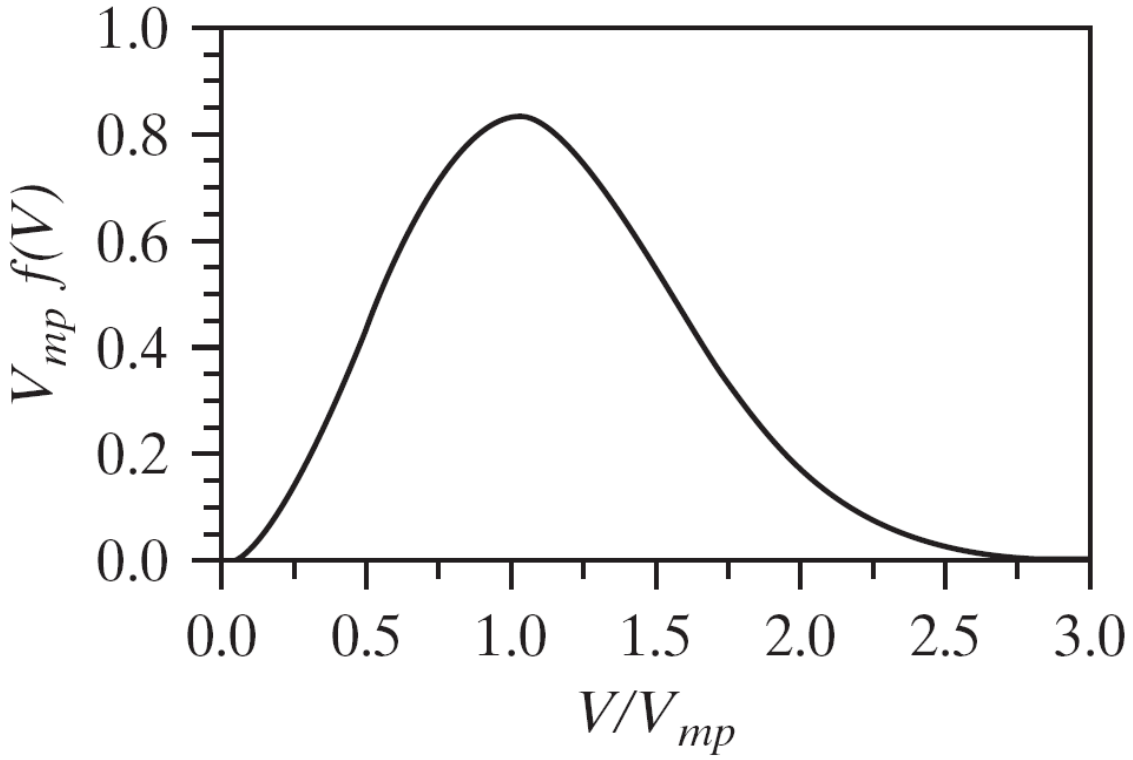

Figure **2-2**: Maxwell Boltzmann speed distribution

Many practical systems can be modeled as if they were composed of independent particles and the examples of this include ideal gases, electrons, radiation and crystalline solid. Hence the Maxwell-Boltzmann distribution can be assumed to hold true for such systems and the following relations hold true for them:

$$KE = \frac{1}{2}\sum_{i=1}^{N} m_i v_i^2 = \frac{3}{2}RT \tag{2.8}$$

where KE is the translational Kinetic Energy of a system of particles which is related to the Temperature T of the system.

2.2.3 Integration Scheme:

In order to evaluate the trajectory of a system of particles, the Newton's equation of motion (2.2) and (2.3) needs to be integrated at each time step using a finite difference method. However, the integration scheme should ensure an accurate, stable and computationally efficient solution. There are several integration schemes available like the Euler scheme[32], Verlet scheme[35], Leap-Frog algorithm[35], Beeman algorithm[35] , Velocity Verlet algorithm[36][37] to name a few. Each of these algorithms uses a Taylor's series expansion to extrapolate the future position and velocity as a function of current position and velocity as shown in equation (2.9) and (2.10)

$$r_i(t+\delta t) = r_i(t) + \frac{dr_i(t)}{dt}\delta t + \frac{d^2 r_i(t)}{dt^2}\frac{\delta t^2}{2!} + \cdots \tag{2.9}$$

$$v_i(t+\delta t) = v_i(t) + \frac{dv_i(t)}{dt}\delta t + \frac{d^2 v_i(t)}{dt^2}\frac{\delta t^2}{2!} + \cdots \tag{2.10}$$

Each algorithm makes a compromise between speed and accuracy to obtain a solution. In this research work we have used the Velocity Verlet algorithm[36][37] to calculate the trajectory, which calculates both position and velocity at the same time with error being $o(\delta t^4)$ and $o(\delta t^2)$ respectively. The expressions for position and velocity at a given time $t + \delta t$ are obtained as shown in (2.11) and (2.12)

$$r_i(t+\delta t) \approx r_i(t) + v_i(t)\delta t + a_i(t)\frac{\delta t^2}{2!} \tag{2.11}$$

$$v_i(t+\delta t) \approx v_i(t) + \frac{a_i(t+\delta t)+a_i(t)}{m}\delta t \tag{2.12}$$

where $v_i(t) = \frac{dr_i(t)}{dt}$ and $a_i(t) = \frac{d^2 r_i(t)}{dt^2}$. Note that, in order to calculate velocity we need to know the forces acting on the particle at next time step i.e $a_i(t+\delta t)$.

The time step δt used in a MD simulation is restricted by the speed of the fastest moving atoms in the system. For example, the vibration frequency of small atoms like H in a bond is of the order of femtoseconds. Hence, in order to account for the accurate motion of atoms, one needs

to use time step of the order of sub femto-seconds. Because of this issue MD simulations are restricted to very small time scale simulations(at best for 1μs), with the currently available computational resources.

2.2.4 Periodic Boundary Conditions:

With the currently available computational resources, MD method can simulate a system of up to $o(10^6)$ atoms, which is far removed from a bulk system. In order to simulate bulk systems, the periodic boundary conditions are chosen which mimic the presence of an infinite bulk surrounding the actual system. The volume containing the system of particles is treated as the primitive cell of an infinite periodic lattice of identical cells as shown in figure 2-3. Hence, the atoms leaving the boundary of the primitive cell, re-enter from opposite face. Any atom in this primitive cell now interacts with all other particles in this infinite periodic system. However, this would mean calculation of infinite terms for getting the interaction potential for every particle in the system. This is avoided by considering only short-range interactions for the particles, and choosing the volume of the primitive cell big enough to make this assumption valid. Usually a cutoff radius $r_c \leq \frac{L}{2}$ is chosen around each particle such that interactions with the particles within this distance are only considered. L is the side length of the primitive cell shown in figure 2-3. This condition ensures that the interactions of a particle are only with the nearest periodic image of other particles. While the assumption of short-range interactions helps improve the speed of MD calculations drastically, correction terms need to be added to the calculated interaction potential of each particle in order to maintain energy conservation.

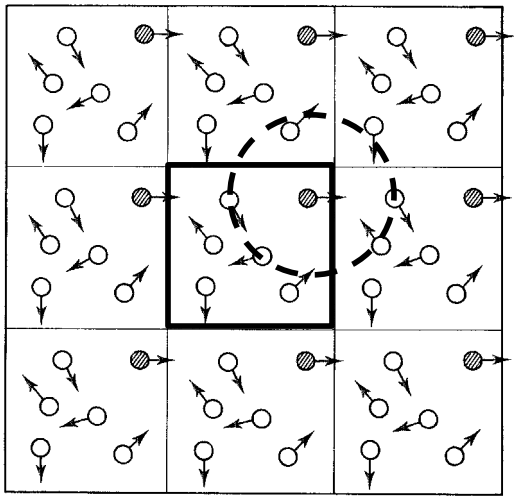

Figure **2-3**: Schematic representation of periodic boundary conditions in two-dimensions.

2.2.5 Interaction Potential:

One of the key factors behind reliability of results from a MD simulation is the choice of interaction potential. In MD we only consider the motion of nuclei of an atom and ignore the electronic motion. We also assume that the dynamics of the system can be represented by Newton's equations of motion. The first assumption holds true under the validity of the Born-Oppenheimer approximation [38].

Born and Oppenheimer observed that the mass of electrons is much less than the nuclei and they move very rapidly as compared to the nuclei. Based on this, they were able to show that the energy of a system of particles can be approximately calculated based only on the nuclei position and velocities and the use of an appropriate potential energy function which incorporates average effects of electronic motion.

As can be seen in equation (2.5), the interaction potential can be classified into three types namely the external potential field, two-body interaction potential and many-body

interaction potential. The interaction between particles for a covalent system can be further classified into bonded and non-bonded interactions. The non-bonded interactions chiefly consist of coulomb forces and van der Waals forces while the bonded interactions for first-row elements typically consist of covalent bonds between two particles and valence angle interactions between three particles and torsion angle interactions between four particles. Equation (2.5) can hence be approximately represented as

$$U = U_{external} + U_{bond} + U_{angle} + U_{torsion} + U_{vdWaals} + U_{Coulomb} \quad (2.13)$$

Interaction potentials can again be broadly classified into two categories, namely non-reactive potentials and reactive potentials. The details of this classification is explained in the following sections.

2.2.5.1 Non-reactive Potential:

Non-reactive potentials usually are relatively simple in form and hence are computationally inexpensive as compared to QM methods. A simple example of a non-reactive potential would be the use of harmonic potential functions to represent bonded interactions, Coulomb's law for non-bonded charge interactions and the 12,6 Lennard Jones potential function[28] for van der Waal's interactions. Because of the simple form of these potential functions, they are easy to parameterize. They can represent the equilibrium structure of a system of particles with good accuracy, but they cannot represent accurate reaction kinetics. For this one requires more complex potential functions, with more parameters which can accurately represent bond formation and dissociation. Some of the popular non-reactive potential functions are AMBER[13] and CHARMM[39], which are widely used for proteins.

2.2.5.2 Reactive Potential:

A reactive potential can simulate reactions between particles by representing the bond formation and dissociation between particles accurately . Unlike, non-reactive potentials, they are able to simulate transition states and barrier energy in a reaction accurately. However, they are computationally more expensive than non-reactive potential methods. Some of the commonly used reactive potentials are ReaxFF[22],AIREBO[18], Brenner[19], Kiefer[20], Tersoff[21] potentials. In our research we will be using the ReaxFF potential functions to perform MD.

2.3 Reactive MD using ReaxFF

ReaxFF is a set of reactive potential functions, which can simulate accurately the formation and dissociation of bonds in a chemical reaction. It is an empirical approach which derives its parameters from smaller scale QM runs and can be run for larger time scales (nano-second scale) and for a large number of atoms(>>1000 atoms), very nearly retaining the accuracy of quantum predictions. Since, its parameters are derived from QM studies, ReaxFF's predictions can be directly applied to systems which cannot be studied experimentally. Unlike other reactive interaction potential functions, ReaxFF does not require prior knowledge of reactive sites. ReaxFF has earlier been applied to a wide range of materials, including organic reactions [22], energetic materials under extreme conduction [40][41], decomposition of explosives [42], thermal decomposition of polymers [43], heterogeneous catalysts [44], fuel cells [45], crack propagation in silicon crystals [46], dissociation of H_2 on Pt surfaces [47], storage of H_2 in magnesium nanoclusters [48], catalytic formation of carbon nanotubes [49], tribology of metal-metal oxide interfaces [50] and hydrocarbon oxidation [51].

2.3.1 Features of ReaxFF:

2.3.1.1 Length and Time scale & Computational Expense:

The length and time scales at which ReaxFF simulates a system of particles is best represented by figure 2.4. While QM methods deal with materials at the smallest length and time scales, continuum methods like Finite element analysis(FEA) deal with materials at a macroscopic length and time scale. ReaxFF deals with materials at an atomistic scale, similar to other empirical potential functions and at a sub femto-second time scale in order to account for high vibrational frequencies of bonds involving small atoms(e.g. Hydrogen atom). In terms of computational expense, ReaxFF scales as $o(n \log n)$ while the faster QM methods scale at best up to $o(n^3)$. However, ReaxFF is around 10-50 times slower than non-reactive potential functions, owing to its complicated potential functions.

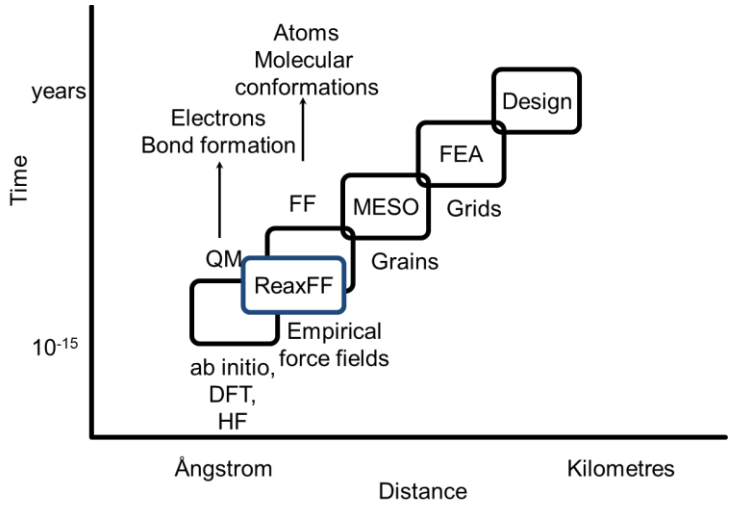

Figure **2-4**: Hierarchy of computational methods for simulating materials on a time vs length scale

2.3.1.2 Bond Order Concept:

ReaxFF employs the concept of bond-order to ensure smooth transition of bond formation and bond dissociation. In the case of harmonic potential functions, the potential energy between two particles goes to infinity when the particles get separated. This is unrealistic and it is the key reason behind non-reactive potentials' inability to simulate reactions. This problem can be avoided if the connectivity dependent potential functions are made dependent on the bond-order, which vanishes to zero when the two particles separate. ReaxFF employs this concept in its potential functions and hence gets a smooth transition in bond formation/dissociation from non-bonded to single, double and triple bonded systems. This also ensures continuity in energy and forces on a particle throughout its trajectory in a MD simulation. This has been illustrated for the carbon-carbon bond in an ethane molecule by comparing the bond energy obtained using Density Functional Theory(DFT, a QM method, see Section 2.4.2), ReaxFF and harmonic potential

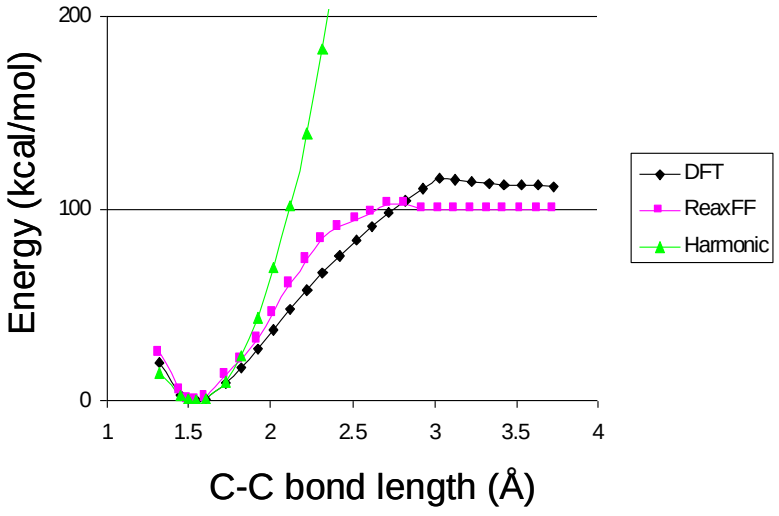

Figure **2-5**: Bond length/bond energy relationship for the C-C bond in ethane according to a harmonic, non-reactive FF (Harmonic), a reactive force field (ReaxFF) and a QM-method (DFT)

function as shown in figure 2.5. Note that around equilibrium bond length, both the harmonic potential and ReaxFF potential describe the bond energy with good accuracy.

The bond-order concept was first introduced by Pauling[52] and has been first implemented in reactive force fields by Tersoff for Silicon[21] and Brenner for hydrocarbons[19]. In ReaxFF, the bond-order is calculated based on the following equation 2.14:

$$BO_{ij} = BO_{ij}^{\sigma} + BO_{ij}^{\pi} + BO_{ij}^{\pi\pi} = \exp\left[p_{bo1}\left(\frac{r_{ij}}{r_o^{\sigma}}\right)^{p_{bo2}}\right] + \exp\left[p_{bo3}\left(\frac{r_{ij}}{r_o^{\pi}}\right)^{p_{bo4}}\right] + \exp\left[p_{bo5}\left(\frac{r_{ij}}{r_o^{\pi\pi}}\right)^{p_{bo6}}\right] \quad (2.14)$$

where r_{ij} is the distance between the particles i and j, $r_o^{\sigma}, r_o^{\pi}, r_o^{\pi\pi}$ are equilibrium bond distance for single, double and triple bond between particles i and j. $p_{bo1}, p_{bo2}, p_{bo3}, p_{bo4}, p_{bo5}, p_{bo6}$ are parameters of the ReaxFF potential function.

The bond-order equation is a continuous function of bond distance and ensures that the bond-order for two particles at infinite separation is zero and gradually increases to single, double and triple bond with decreasing bond distance. Also ReaxFF describes partial bonds, through bond order values less than unity, enabling ReaxFF to simulate transition state structures. This is shown illustratively for a carbon-carbon bond in figure 2-6.

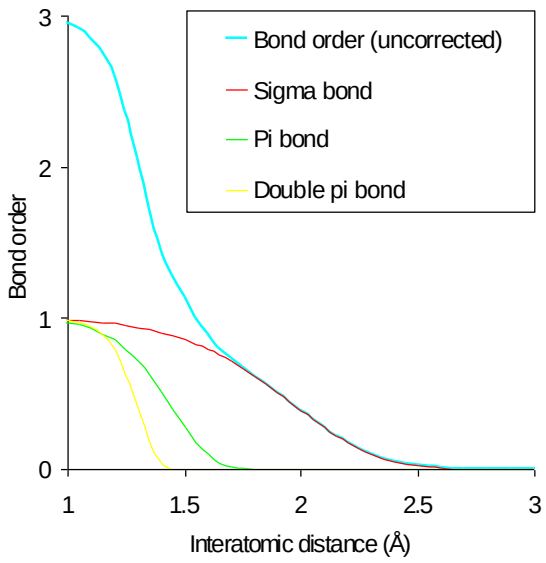

Figure **2-6**: ReaxFF total bond order and sigma, pi and double-pi bond carbon-carbon bond order as a function of interatomic distance.

The chemical reactivity of an atom is dependent on its co-ordination with other atoms. If an atom is fully co-ordinated, then it is in its ground state and the attractive covalent interactions with other atoms(other than the ones it is co-ordinated with) decay quickly, while for an under co-ordinated radical atom the attractive interactions have a longer range. This is due to the free electrons in the outer shell of a radical atom. This effect is incorporated in ReaxFF by introducing a bond-order correction scheme, which corrects the initial bond-order calculated for an atom based on its level of under-coordination. Hence, for an atom whose bond-order exceeds the number of valence electrons, the strong bond-orders are kept intact and all the weak bond-orders are reduced in magnitude. This is not done for under-coordinated radical atoms, ensuring the high reactivity of radicals as compared to ground state molecules. This bond-correction scheme enables ReaxFF to properly capture transition state energies and accurately predict reaction kinetics, as will be shown in our results in Chapter-3.

2.3.1.3 Bonded Interaction Potential functions:

The generalized potential energy terms used by ReaxFF is similar to equation 2.13. However, for H_2/O_2 mixtures additional terms of lone-pair potential energy(due to lone pair present in O_2 molecule) and hydrogen-bonding potential are used.

The bonded-interaction potential functions in ReaxFF are functions of Bond-orders as discussed in section 2.3.1.2 above. The pair-wise bonded interaction potential used in ReaxFF is given as:

$$U_{bond} = -D_e^{\sigma} BO_{ij}^{\sigma} \exp\left[p_{be1}\left(1 - \left(BO_{ij}^{\sigma}\right)^{p_{be2}}\right)\right] - D_e^{\pi} BO_{ij}^{\pi} - D_e^{\pi\pi} BO_{ij}^{\pi\pi} \qquad (2.15)$$

where $D_e^{\sigma}, BO_{ij}^{\sigma}$ represent dissociation energy and bond-order for sigma bond between atom i and j and correspondingly D_e^{π}, BO_{ij}^{π} for a double bond and $D_e^{\pi\pi}, BO_{ij}^{\pi\pi}$ for a triple bond. p_{be1}, p_{be2} are parameters of the potential function. Similar bond-order dependent potential functions have been defined for U_{angle} & $U_{torsion}$ functions.

2.3.1.4 Non-bonded Interaction Potential functions:

Non-bonded interaction terms in ReaxFF are independent of bond order. However, unlike non-reactive potentials, ReaxFF calculates non-bonded interactions between bonded particles as well. The van der Waals interactions in ReaxFF is obtained using a modified Morse potential function, while the charge interactions are obtained using Coulomb's law. Excessively close-range non-bonded interactions are avoided by using a shielding term. The charges on each particle are calculated using a geometry-dependent scheme derived from EEM[53] and Qeq methods[54]. This charge calculation scheme is the most expensive part of ReaxFF in terms of computational speed.

For a full description of all the potential functions used in ReaxFF and their corresponding parameters, please refer to the supporting material of Chenoweth et al [51].

2.3.1.5 Transferability and training:

With the reactive potential functions of ReaxFF it is possible to describe covalent, metallic and partially ionic materials and it has been used to simulate physical and chemical behavior of elements all across the periodic table. In order to use ReaxFF to describe a certain material or a set of materials, its parameters need to be optimized against a mainly QM derived database (the 'training set') which describes all the molecular and material properties. These properties include atomic charges, bond dissociation energies, angle strain, heats of formation, vibrational frequencies and transition-state energies.

The parameters of the ReaxFF potential functions are optimized for a certain material through a single parameter search optimization [55] performed using the training set, to minimize the following sum of squares:

$$\text{Error} = \sum_{i=1}^{n} \left[\frac{\left(x_{i,QM} - x_{i,ReaxFF}\right)}{\sigma} \right]^2 \tag{2.16}$$

where $x_{i,QM}$ represents the QM calculated value and $x_{i,ReaxFF}$ the ReaxFF calculated value of the data fed in the training set. σ represents the desired accuracy specified in the training set.

The QM data for the training set used for the H_2/O_2 system has been obtained through Density Functional Theory(DFT) calculations using the Jaguar code(version 7.5)[56].The DFT method used was B3LYP[57][58] and the basis used was the Pople 6-311G** basis set [59].Also some of the heat of formation data has been obtained through G3 energy values of Pople et al [60][61][62][63].

2.4 Quantum Mechanics

2.4.1 Basics of Quantum Mechanics(QM)

As discussed previously, the success of MD, in simulating a system of particles is dependent on the quality of interaction potential used, which in turn depends on the quality of the training set which is used to optimize the potential functions. Therefore we use QM derived data in the training set.

QM is the most accurate method known to researchers till date, for determining energy and structure information for a system of atoms, using the steady-state Schrodinger equation

$$\hat{H}\psi(x,y,z) = \varepsilon\psi(x,y,z) \tag{2.17}$$

where $\hat{H}$ is defined as the Hamiltonian operator which corresponds to the classical Hamiltonian

$$H = T + V \tag{2.18}$$

where T is the kinetic energy and V is the potential energy of the system. ψ is the wave function which defines the state of the system such that the quantity $\psi^*\psi dxdydz$ gives the probability of position vector (x,y,z) of a particle lying within (x,y,z) and $(x+dx, y+dy, z+dz)$. ε is the energy of the system. For any dynamic variable A a linear hermitian operator $\hat{A}$ is defined such that the average value of A can be obtained as

$$\langle A\rangle = \int \psi^* \hat{A}\psi \, dxdydz \Big/ \int \psi^*\psi \, dxdydz \tag{2.19}$$

Equation(2.17) is an eigen value problem which always gives real values of energy ε.However, the Hamiltonian operator $\hat{H}$ of a system of particles is often very complex and makes it computationally rigorous to solve. Therefore approximations have been made to solve this equation using approximate methods like Hartree-Fock[64] and Density functional theory[64] which are designed to alleviate the computational complexity. In order to train parameters of

ReaxFF potential function, we have used the density functional theory method to obtain QM energy values for our system of study i.e. H_2/O_2.

2.4.2 Density Functional Theory(DFT)

Density functional theory is a computational method which derives properties of a system of particles based on the determination of 'electron density' of the system. The idea first originated from Thomas and Fermi who found a one-to-one correspondence between wavefunction of a many-electron molecule and its electron density. DFT basically refers to expressing the energy of the system as a 'functional' of electron density, which is a function of only three variables i.e. x,y,z co-ordinates. Solving for the wave function of a many electron system using the Schrodinger equation is very complicated and becomes more complicated with each extra electron. The electron density determination on the other hand is expressed as a linear combination of a basis set of functions whose co-effiecients are determined from simplified wave functions, depending on the DFT method being used. DFT is a general purpose computational tool and can be applied to a wide range of systems. Its computational complexity is $o(n^3)$ where n is the number of basis functions used.

DFT methods can be classified into three types: (1) Local Density Approximation (LDA) methods, (2) methods with Gradient-correction factor and (3) hybrid methods which incorporate a combination of Hartree-Fock and DFT approximation to electron-exchange energy. The hybrid methods are currently the most frequently used DFT methods, the B3LYP[57][58] method being the most popular among them. The B3LYP method is good for organic molecules, but not as good for metal-containing compounds. It is considered to be the 'industry standard' in terms of practical applications. For all these reasons, we have chosen the B3LYP method for our QM calculations on H_2/O_2 system. The basis set we used was Pople's 6-311G**[59] which is a

polarized split-valence basis set and combined with the B3LYP method is considered on an average to be the best choice of a model chemistry for most systems.

Chapter 3

ReaxFF Force-Field Development

3.1 Building the FF Training Set

In order to obtain a ReaxFF FF which predicts accurately all the aspects of H_2/O_2 chemistry, we required adequate data to train the parameters of ReaxFF FF. First and foremost we added the standard heat of formation values of key reaction components of hydrogen combustion (i.e. H, O, OH, HO_2, H_2O_2 and H_2O). The values added in the training set are obtained from G3 energy calculations of Pople et al[60][61][62][63]. We also added the heat of reaction and activation energy of all the important reactions in H_2/O_2 chemistry as given in Li et al [9], in the training set. Besides this, we added QM data related to pair-wise bonded interactions, three-body bonded interactions and four-body bonded interactions. The training set also includes partial charges on atoms of polarized molecules like H_2O.

Data related to pairwise interactions consist of H-H bond dissociation curve, O-O bond dissociation curve, O=O bond dissociation curve and O-H bond dissociation curve. Data related to three-body interactions consist of valence angle distortion around equilibrium angle of H-O-H angle in H_2O, H-O-O angle in H_2O_2. The ground state energy of each bond and valence angle was calculated through full geometry optimization. Other points on the bond dissociation curve and angle distortion curve were obtained by restraining the internal co-ordinates of interest and optimizing the rest of the geometry. Four body interaction terms include interaction of two hydrogen molecules close to each other.

In addition, the training set consists of transition states of reactions as a function of the angle of approach of the reactants. For example, consider the reaction

$H_2 + O_2 \rightarrow H + HO_2$ (R15)

The reactants H_2 and O_2 are made to approach each other such that the H-O-O angle is kept fixed and the reactants approach each other to react and form the products. This process is repeated for angles varying from 80-180 degrees. For each angle, the transition state structure formed is of a different energy and hence the activation energy is different. Adding such data into the training set will make sure that ReaxFF can reproduce the whole potential energy surface with good accuracy, and hence simulate accurate reaction kinetics.

To properly describe the H_2/O_2 chemistry, a change was made in the lone pair potential function of ReaxFF from its earlier version. This was necessary because ReaxFF was not able to predict the heat of reactions of the following reactions correctly:

$H_2O \rightarrow H + OH$ (R16)

$OH \rightarrow O + H$ (R17)

While both R16 and R17 involve the breaking of a single O-H bond, the O-H bond in R17 is easier to break because of lone pair stabilization on the O radical formed. Hence, to account for this effect the lone pair potential in ReaxFF has been modified. In the earlier versions of ReaxFF, the lone pair potential function used is as given below:

$$U_{lp} = \frac{p_{lp2}\Delta_i^{lp}}{1+\exp\left(-75\Delta_i^{lp}\right)} \quad (3.1)$$

Where,

$$\Delta_i^{lp} = n_{lp,opt} - n_{lp,i} \quad (3.2)$$

$$n_{lp,i} = int\left(\frac{\Delta_i^e}{2}\right) + \exp\left(-p_{lp,1}\left(2 + \Delta_i^e - 2 * int\left\{\frac{\Delta_i^e}{2}\right\}\right)^2\right) \quad (3.3)$$

$$\Delta_i^e = -Val_i^e + \sum_{j=1}^{neighbors(i)} BO_{ij} \quad (3.4)$$

In eq(3.4) Val_i^e is the total number of free electrons in the outer shell of atom i and $n_{lp,i}$ determines the available lone-pairs on atom i based on the number of bonds made by the atom. A penalty energy given by eq(3.1) is applied on the atom if $n_{lp,i}$ is different from the optimal

number of lone pairs on the atom given by $n_{lp,opt}$. p_{lp1}, p_{lp2} are parameters of the potential function. The optimal number of lone pairs on the atom is obtained from the relation

$$n_{lp,opt} = 0.5 * (Val_i^e - n_{val,i}) \quad (3.5)$$

Where $n_{val,i}$ is the valency of atom i (e.g. 2 for O, 1 for H, 4 for C).

In the new lone pair potential function equation(3.5) is modified to take into account the fact that without any bonds, an atom can make an extra lone pair(e.g. O atom without neighbors can have 3 lone pairs). Hence to account for this, equation (3.5) is modified to

$$n_{lp,opt} = 0.5 * \left(Val_i^e - n_{val,i}\right) + vpar2 \quad (3.6)$$

where $vpar2$ is an atom force field parameter.

The parameters of the ReaxFF force field were optimized using the above training data, using the method described in section 2.3.1.5 of chapter 2.

3.2 Validation

After the ReaxFF FF is optimized its accuracy was determined by evaluating the goodness of the fit obtained by the FF training. In order to do this, the optimized FF predictions are compared to the training set data.

3.2.1 Heat of Formation & Heat of Reaction:

The heat of formation (at 0K) values of key reaction components of hydrogen combustion as obtained from ReaxFF are in very good agreement with QM calculated values . Table 3-1 shows the comparison between QM and ReaxFF. The highest deviation in ReaxFF predictions is within 6 kcal for H_2O_2.

The heat of reactions of all the key reactions of a hydrogen/oxygen mixture as calculated in ReaxFF is shown in Table 3-2. These reactions have been taken from Li et al.[9], and were quoted as the important reactions in hydrogen combustion by Mueller et al.[8] and earlier by Yetter et al.[65]. Table 3-2 shows a comparison of the heat of reactions and activation energies between ReaxFF and literature values (obtained from experiments). We can notice good agreement for heat of reactions, with maximum deviation of ~10 kcal for reaction 13 in Table 3-2. The activation energies are also in good agreement with maximum deviation of ~8 kcal for reaction 6 in Table 3-2.

Table **3-1**: Comparison of Standard heats of formation at 0K of key species of Hydrogen Combustion in QM and ReaxFF.

ΔH^0_f (0K) (kcal)	ReaxFF	Quantum
H	51.54	51.89
O	59.19	58.43
OH	7.35	8.4
H_2O	-51.59	-56.8
H_2O_2	-35.28	-29.9
HO_2	1.67	3.13

3.2.2 Bond Dissociation Curve:

Figures 3-1,3-2,3-3,3-4 and 3-5 show the bond dissociation curves obtained for H-H bond in H_2, O-H bond in H_2O,O-O double bond in O_2,O-O single bond in H_2O_2 , O-O single bond in HO_2 respectively for ReaxFF and QM. As seen in Figure 3-1, the point at zero energy represents the ground state energy of the bond. The portion where the curve starts to flatten out represents the dissociation limit for the bond. For the dissociation curve of the O-O single bond in HO_2

Table **3-2**: Comparison of Standard heats of Reaction and Activation Energy of key reactions of Hydrogen Combustion in literature and ReaxFF.All Energies are in kcal.

	Reactions	$\Delta H_r^0{}_{0K}$ (ReaxFF)	$\Delta H_r^0{}_{298K}$ (Baulch et al [66])	Ea (ReaxFF)	Ea (Li et al [9])
	Chain Reactions				
1	$H + O_2 \rightarrow O + OH$	15.00	16.31	19.76	16.6
2	$O + H_2 \rightarrow H + OH$	-0.30	1.41	6.72	6.29
3	$H_2 + OH \rightarrow H_2O + H$	-7.40	-14.56	0	3.43
4	$H_2O + O \rightarrow OH + OH$	7.11	15.95	11.81	13.4
	H_2/O_2 Dissociation/Recombination Reactions				
5	$H_2 + M \rightarrow H + H + M$	103.08	104.11	105.28	104.38
6	$O + O + M \rightarrow O_2 + M$	-118.37	-119.1[a]	7.91	0[b]
7	$O + H + M \rightarrow OH + M$	-103.38	-102.3[a]	0	0
8	$H + OH + M \rightarrow H_2O + M$	-110.48	-118.68	0	0
	Formation/Consumption HO_2				
9	$H+O_2+M \rightarrow HO_2+M$	-49.87	-48.342	0	--
10	$HO_2 + H \rightarrow H_2 + O_2$	-53.21	-55.562	5.36	0.82
11	$HO_2 + H \rightarrow OH + OH$	-38.51	-37.832	0	0.3
12	$HO_2 + O \rightarrow OH + O_2$	-53.51	-53.362	0	0
13	$HO_2 + OH \rightarrow H_2O + O_2$	-60.62	-70.362	0	--
	Formation/Consumption H_2O_2				
14	$HO_2 + HO_2 \rightarrow H_2O_2 + O_2$	-38.62	-39.052	0	--
15	$OH + OH + M \rightarrow H_2O_2 + M$	-49.98	-50.282	1.23	--
16	$H_2O_2 + H \rightarrow H_2O + OH$	-60.51	-68.412	0	3.97
17	$H_2O_2 + H \rightarrow H_2 + HO_2$	-14.59	-16.032	3.99	7.95
18	$H_2O_2 + O \rightarrow OH + HO_2$	-14.89	-14.312	3.73	3.97
19	$H_2O_2 + OH \rightarrow H_2O + HO_2$	-21.99	-30.332	0	--

[a] refers to values taken from Mueller et al [8]

[b] $M \neq Ar,He$

(figure 3-5) we have calculated multiple spin states in QM. This is because the quartet state calculations yield lower energy values compared to doublet state when O-O bond is near the dissociation limit. Since ReaxFF does not include the concept of multiple spin states and is parameterized to reproduce the energy corresponding to lowest energy state, we have added quartet state energy values for large separation distance of O-O bond and doublet energy values near equilibrium bond distance.

Besides these bond dissociation curves we also incorporated QM data for bond dissociation in the following hydrogen exchange reactions:

$$H_A - H_B + H_C \rightarrow H_A + H_B - H_C \quad \text{(R18)}$$

$$H_A - H_B + H_C - H_D \rightarrow H_A - H_C + H_B - H_D \quad \text{(R19)}$$

Figure 3-6 and 3-7 show comparison between ReaxFF and QM for reactions R18 and R19 respectively.

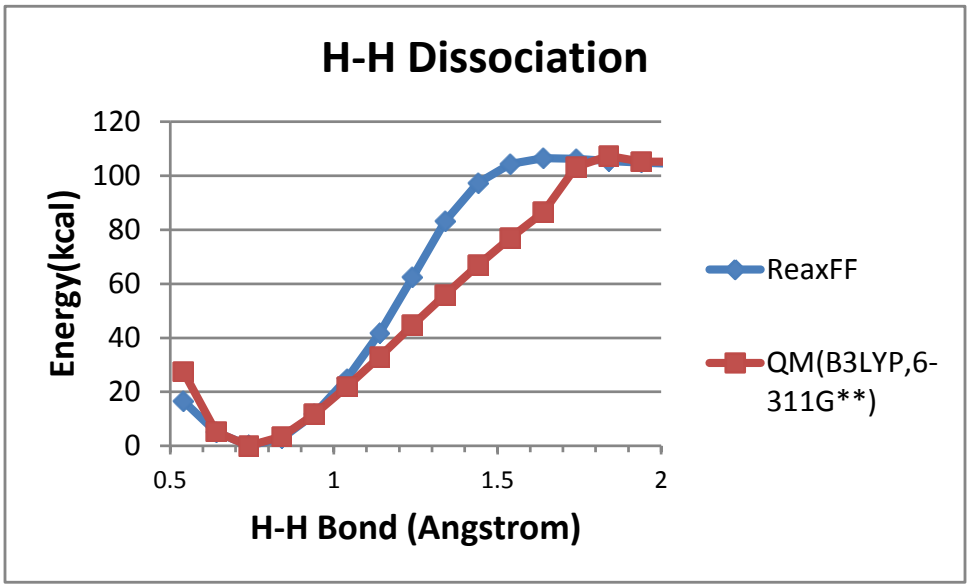

Figure **3-1**: QM(B3LYP/6-311G**) and ReaxFF bond dissociation energies for H-H single bond in H_2.

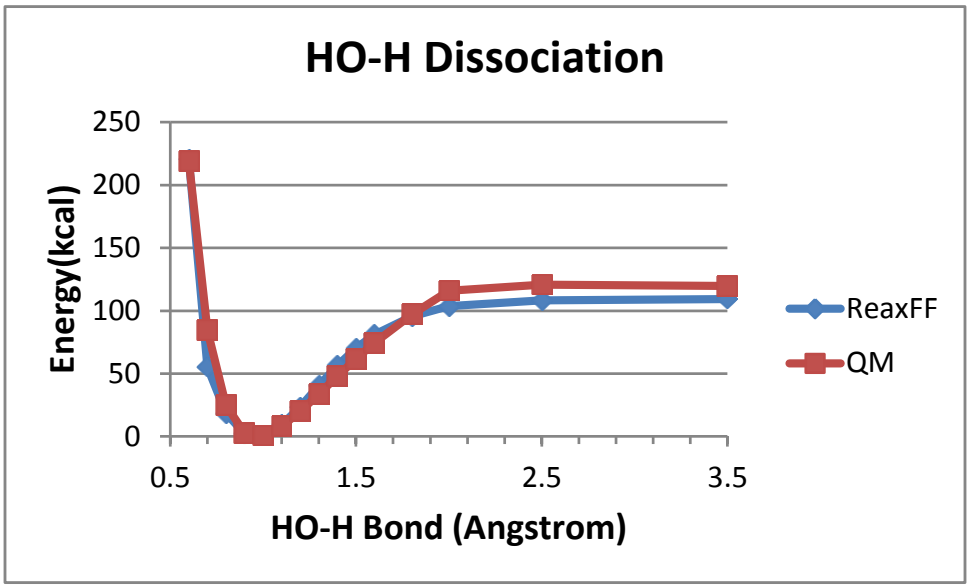

Figure **3-2**: QM(B3LYP/6-311G**) and ReaxFF bond dissociation energies for O-H single bond in H_2O.

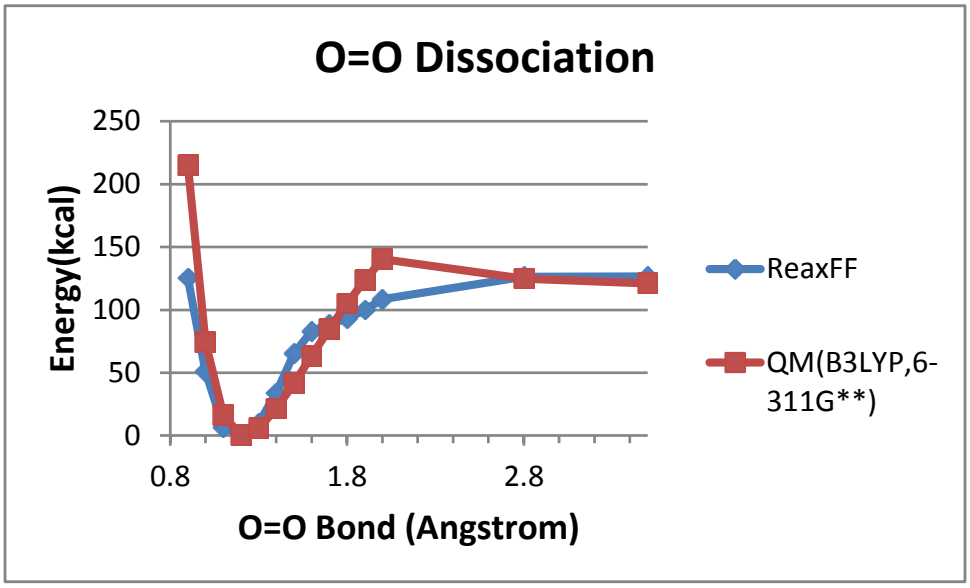

Figure **3-3**: QM(B3LYP/6-311G**) and ReaxFF bond dissociation energies for O-O double bond in O_2.

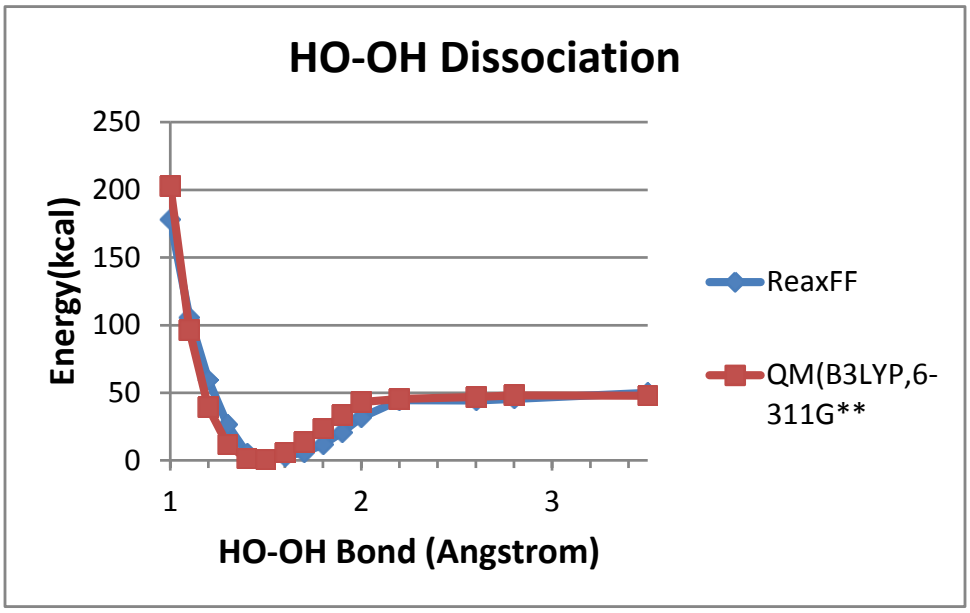

Figure **3-4**: QM(B3LYP/6-311G**) and ReaxFF bond dissociation energies for O-O single bond in H_2O_2)

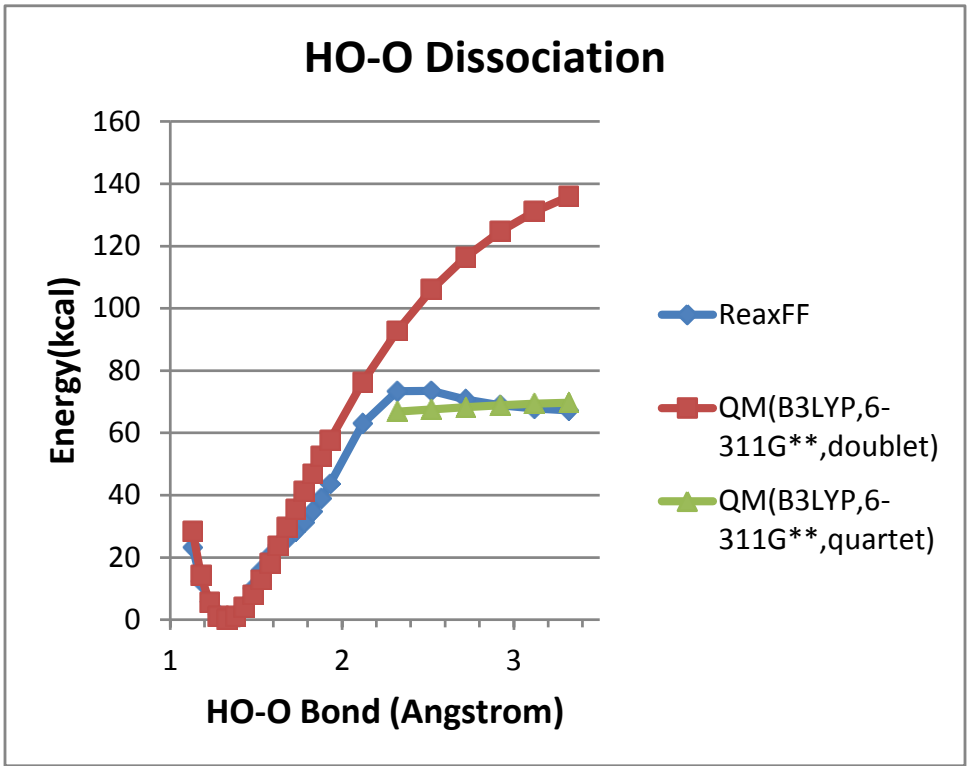

Figure **3-5**: QM(B3LYP/6-311G**) and ReaxFF bond dissociation energies for O-O single bond in HO_2

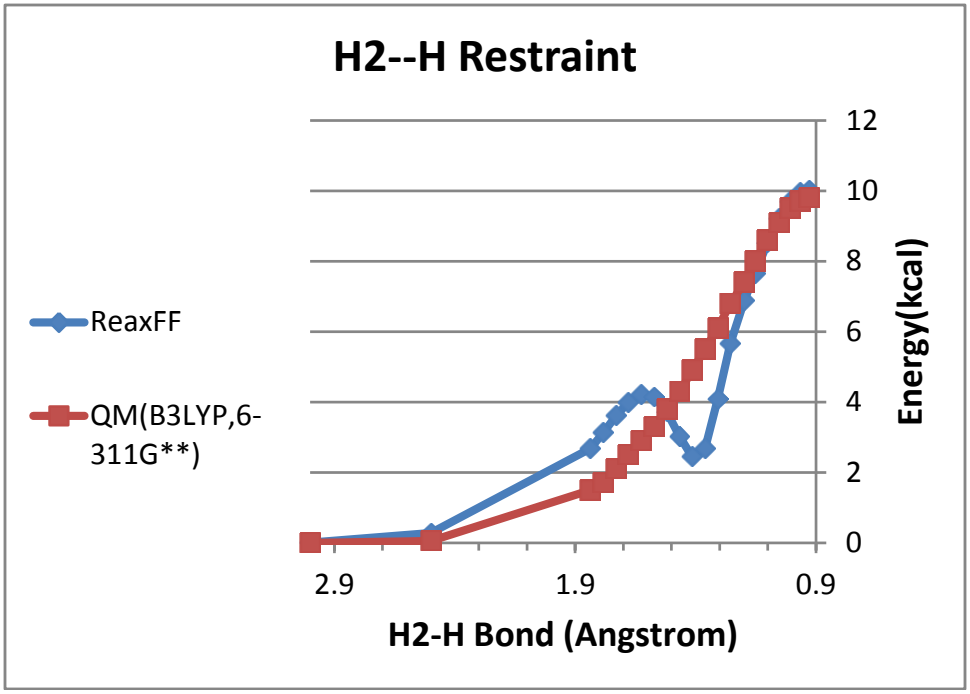

Figure **3-6**: QM(B3LYP/6-311G**) and ReaxFF bond dissociation energies for H_A-H_B + H_C → H_A + H_B-H_C

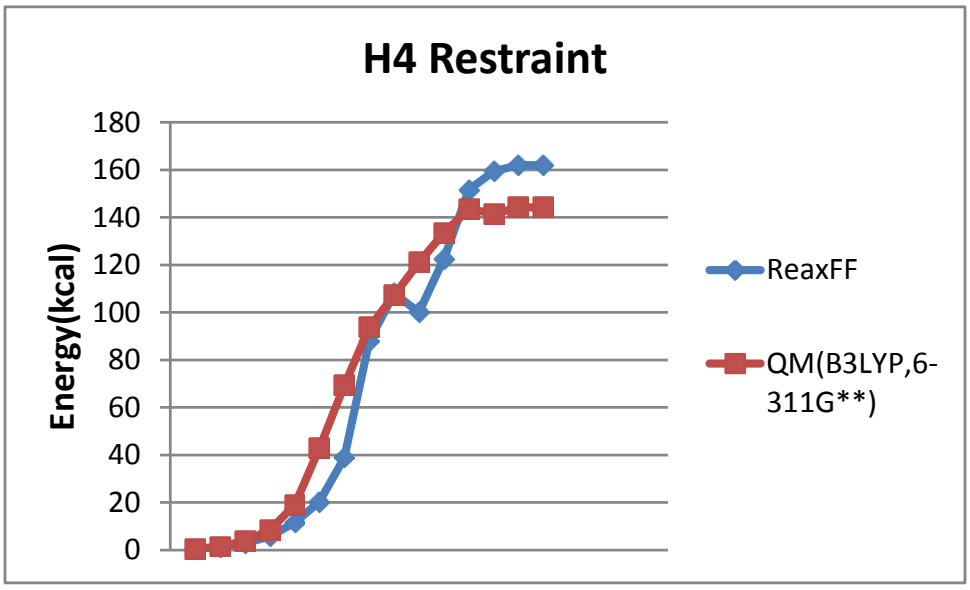

Figure **3-7**: QM(B3LYP/6-311G**) and ReaxFF bond dissociation energies for H_A-H_B + H_C-H_D → H_A-H_C + H_B-H_D

3.2.3 Angle Distortion Curves:

Figure 3-8, 3-9 show the angle distortion energy curves for H-O-H angle in water and H-O-O angle in hydrogen peroxide. In figure 3-9 we see that ReaxFF captures the trend of H-O-O angle distortion as predicted by QM, however the ground state angle in ReaxFF shifts from 100^0 to 106^0. We could have improved the ReaxFF prediction by increasing the required accuracy for H-O-O angle as mentioned in equation 2.16. However, making it more accurate resulted in loss of accuracy of transition state energy of the H atom of HO_2 radical switching from one O atom to another. Given our application target we deemed that this transition state energy was more important than the H-O-O angle equilibrium value; as such we accepted this deviation between ReaxFF and QM.

3.2.4 Activation Energies:

Figure 3-10 and 3-11 show the transition state energies as a function of a valence angle between the reactants of the reactions R15 and R20.

$H_2+O_2 \rightarrow H + HO_2$ (R15)

$H_2O + O \rightarrow 2OH$ (R20)

In R15, the H-O-O valence angle between the H_2 and O_2 molecule is constrained and in R20 the O-H-OH angle between O radical and H_2O molecules is constrained. Figure 3-10 shows that the ReaxFF predictions of activation energy match pretty well with QM predictions with a maximum deviation within 22 kcal, for an unlikely angle of approach. Figure 3-11 shows the comparison between QM calculations and ReaxFF predictions with a maximum deviation observed to be approximately 20kcal, again for an unlikely angle of approach.

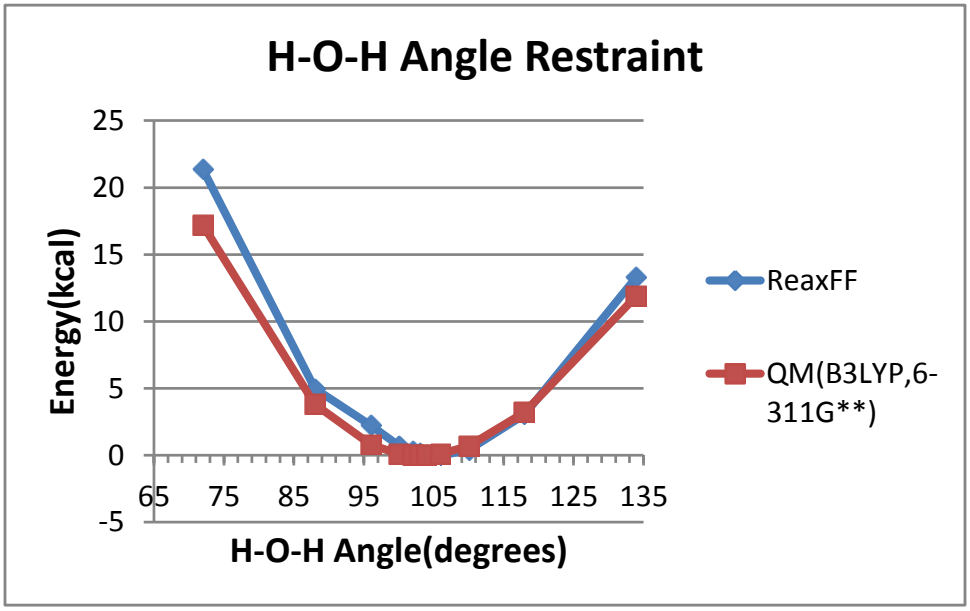

Figure **3-8**: QM(B3LYP/6-311G**) and ReaxFF energy for distortion of H-O-H angle in H_2O.

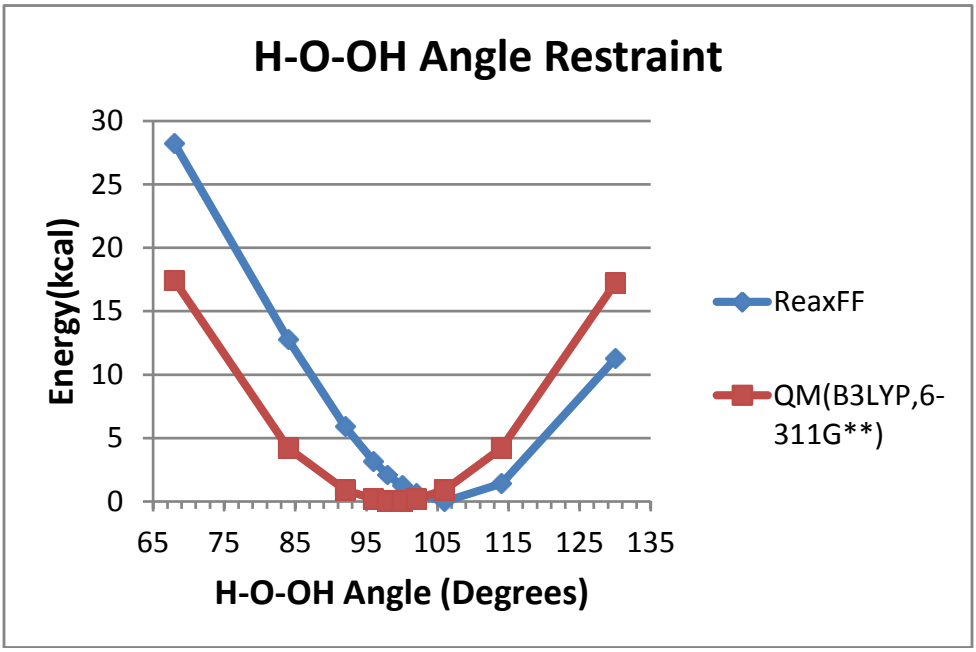

Figure **3-9**: QM(B3LYP/6-311G**) and ReaxFF energy for distortion of H-O-O angle in H_2O_2

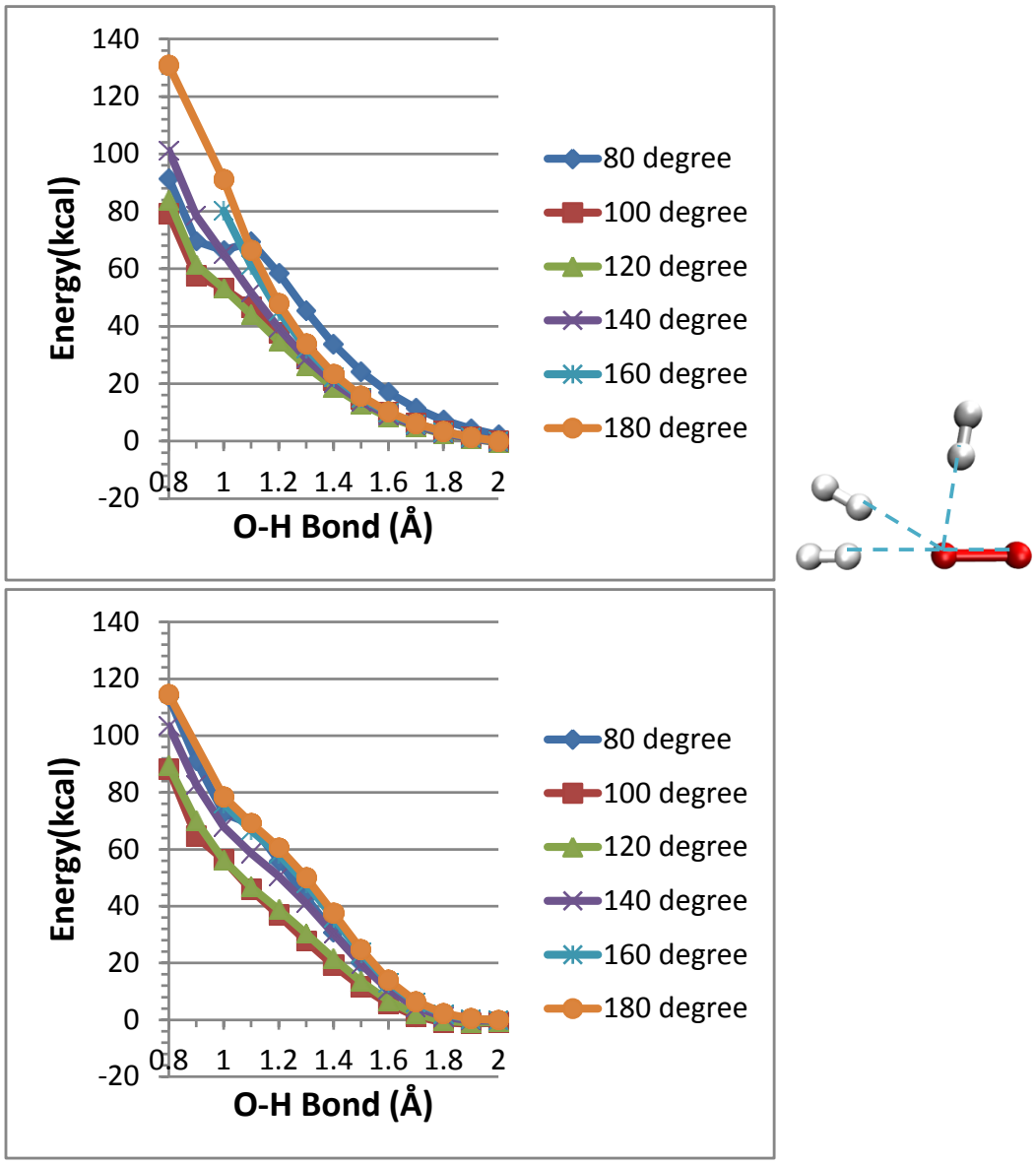

Figure **3-10**: QM(B3LYP/6-311G**)(up) and ReaxFF(down) energy for distortion of H-O-O angle when H_2 molecule approaches a O_2 molecule. For each H-O-O angle, the energies are shown as a function of the O-H bond formed between the approaching O and H atom of O_2 and H_2 respectively. The figure on the right side shows the H-O-O angle formed between H_2(white) and O_2(red).

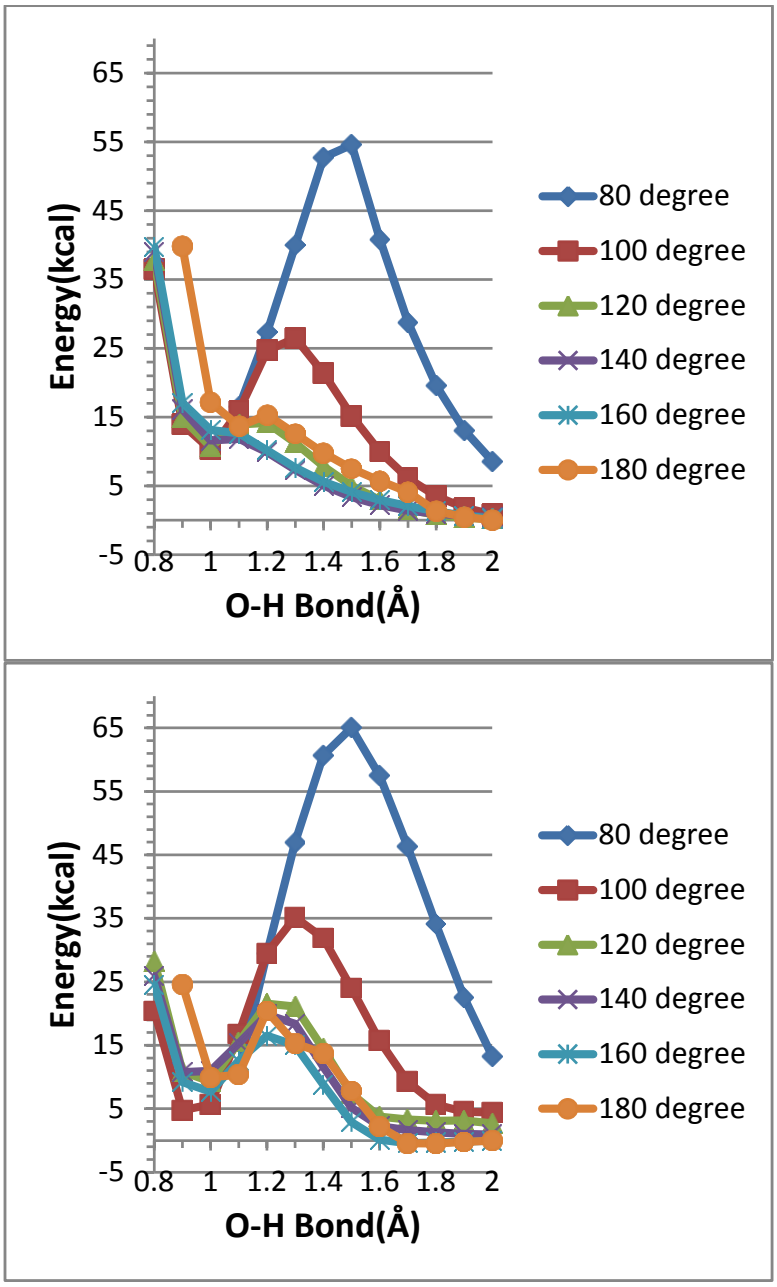

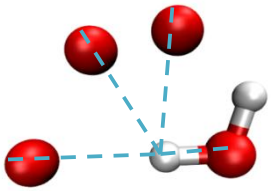

Figure **3-11**: QM(B3LYP/6-311G**)(up) and ReaxFF(down) energy for distortion of O-H-OH angle when O radical approaches a H atom in H_2O molecule. For each O-H-OH angle, the energies are shown as a function of the O-H bond formed between the approaching O radical and H atom. The figure on the right side shows various O-H-OH angles formed(O atoms are red and H atoms are white).

A more comprehensive validation of potential energy surface prediction was done for reaction R21.

$H_2 + O \rightarrow OH + H$ (R21)

The activation energy of this reaction was evaluated in QM and ReaxFF for all possible reaction coordinates. Reaction R21 essentially involves the formation of an O-H bond and dissociation of an H-H bond. For this reaction we considered a 2D grid of bond lengths, considering the H-H bond distance and O-H bond distance as the co-ordinates of the grid(Figure 3-12). We created geometries for each grid point and energy minimized them in QM (by constraining the bond lengths of interest and optimizing the rest of the geometry). The left top grid point in figure 3-12 represents the starting point of the reaction R21.This point is taken as the zero energy point. The right bottom point of the grid is considered the end point of reaction. Figure 3-12 shows the reaction energy comparison in QM and ReaxFF. The black line in QM and ReaxFF plot show the corresponding lowest energy path observed. QM predicts a barrier of 9.5 kcal along lowest energy path, while ReaxFF predicts a barrier of 6.7 kcal.

3.2.5 Validation from MD results:

In order to further validate the force field, we conducted one MD simulation with the optimized force field, which is an NVT MD simulation of 200 atoms, containing 67 H_2 molecules and 33 O_2 molecules at 3500K. From this MD simulation trajectory, we randomly picked molecule geometries of key reaction components of hydrogen combustion (i.e. H_2, O_2, H_2O, OH and HO_2) from various instants of the simulation. Using these geometries we calculated their standard heat of formation (at 0K) in ReaxFF and QM based on their single-point energies.

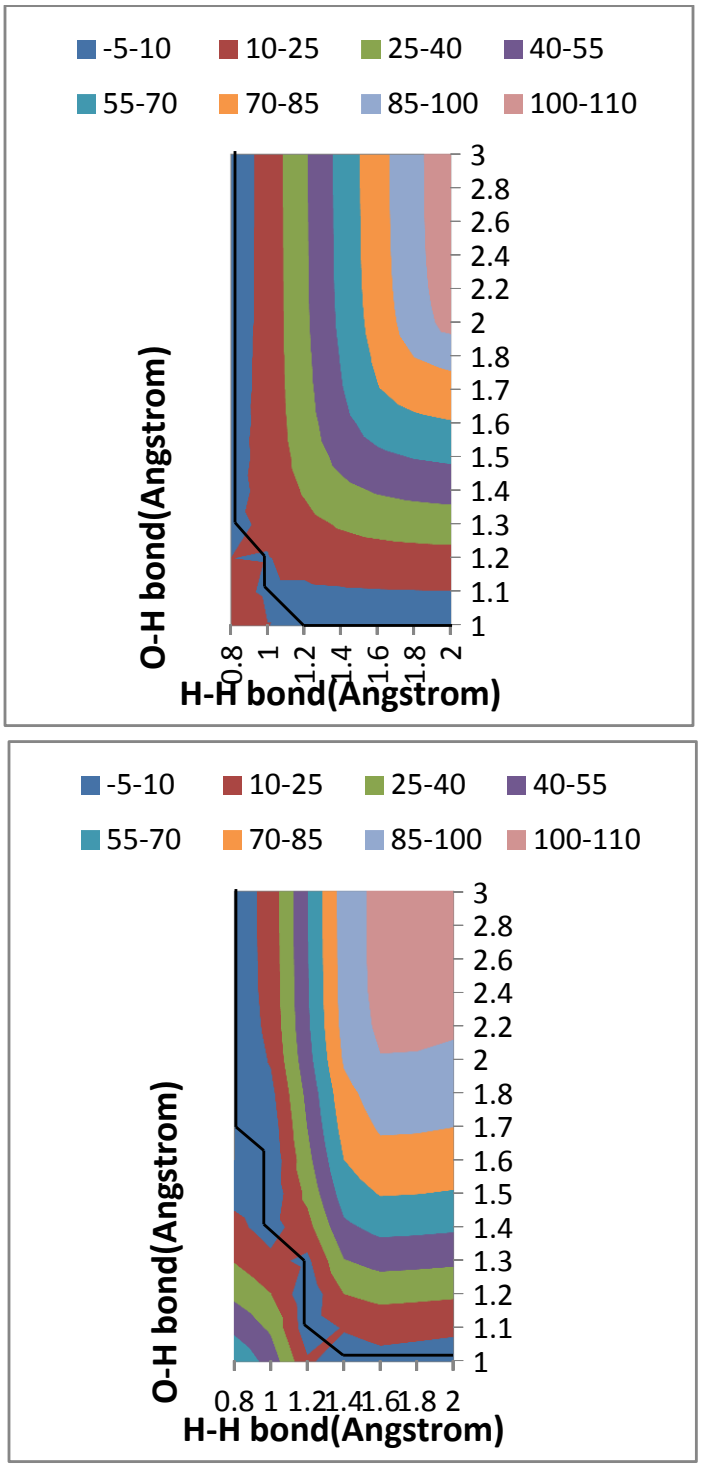

Figure **3-12**: QM(B3LYP,6-311G**)(up) and ReaxFF(down) energy(in kcal) for the reaction H_2+O→OH+H .Starting with H_2 and O, the O-H and H-H distances are varied along a 2D grid of O-H and H-H bond distance, till the products OH and H atoms are formed. The black line on the contours represent the lowest energy path.

Figure 3-13 shows a comparison between QM and ReaxFF predictions. We observe that the heat of formation of ground state molecules like H_2, O_2 and H_2O are predicted with good accuracy, compared to QM, while there is more deviation in case of reaction intermediates like OH and HO_2 radicals. This is likely because our training set chiefly consists of data related to ground state molecules, while the reaction intermediates are only described in the transition state data. However, this analysis enables us to identify areas where the force field is less accurate, which enables us to further improve the quality of the force field in the future by adding corresponding structures in the training set with QM calculated values.

Having validated the force field comprehensively, we were in good shape to use this ReaxFF FF to conduct MD simulations and analyze the reaction chemistry of H_2 and O_2. Appendix A contains a list of the final force field parameters.

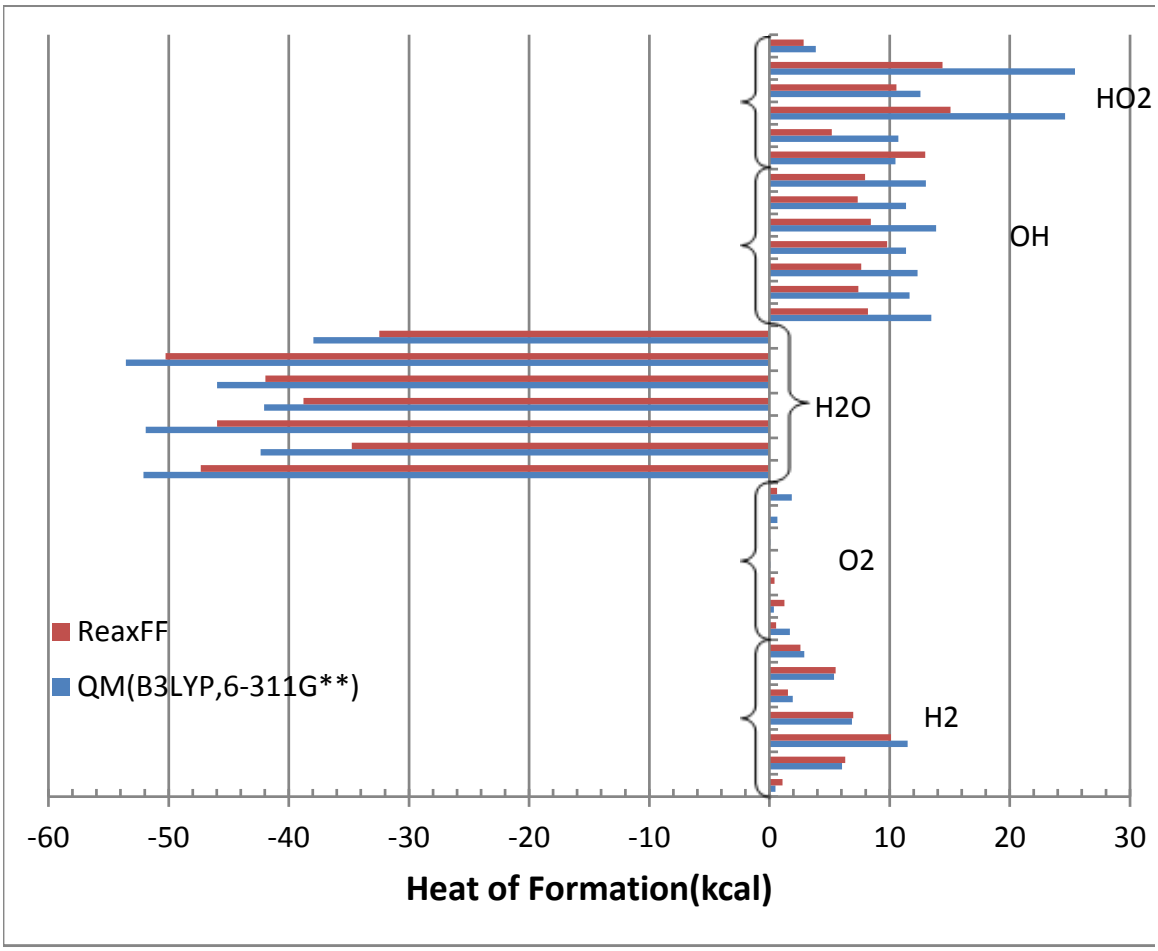

Figure **3-13**: QM(B3LYP,6-311G**) and ReaxFF calculated heat of formation at 0K for molecules obtained randomly from a NVT MD simulation run for 500ps at 3500K in a cubic periodic box of side length 25Å containing $67H_2$ and $33O_2$ molecules.

Chapter 4

MD using ReaxFF

Molecular dynamics simulations of H_2 and O_2 mixtures were performed for a wide range of input conditions using ReaxFF. The simulations are performed for a canonical ensemble with constant number of atoms (N) in a cubic periodic box of constant volume (V) at a constant temperature (T). These conditions are commonly referred to as NVT. A summary of all input conditions used in our research can be seen in Table 4-1.

4.1 Methodology

The simulation procedure begins with placing H_2 and O_2 molecules in a periodic box and energy minimizing the resulting structure (using the Shanno conjugate gradient method [67]). After this every atom in the box is assigned a random velocity and the temperature of the system is slowly ramped up to the desired temperature. Once the desired temperature is attained, simulations are continued for around 0.5 nano seconds. The trajectory of the atoms is calculated using Velocity-Verlet scheme[36][37] as discussed in section 2.2.3 of chapter-2. The time step used in all our simulations is 0.1 fs. The temperature of the system is controlled using a Berendsen thermostat[29] as discussed in section 2.2.2.3 of chapter-2. The temperature damping constant used was 500 fs. Each MD simulation run using ReaxFF on an average takes 6 hours CPU time on a single processor with clock speed 3GHz. Snapshots of one of the NVT simulations run at 3500K with 67 H_2, 33O_2 molecules in a cubic periodic box of side length 25Å are shown in figure 4-1 and 4-2.

Table **4-1**: Number of atoms,Temperature, Density and Equivalence ratio of the systems studied

Ensemble	Number of Atoms (N)	Temperature(K)	Density(kg/dm^3)	Equivalence Ratio(Φ)
NVT	200	2750-4000	0.03-0.25	0.25 – 4.50

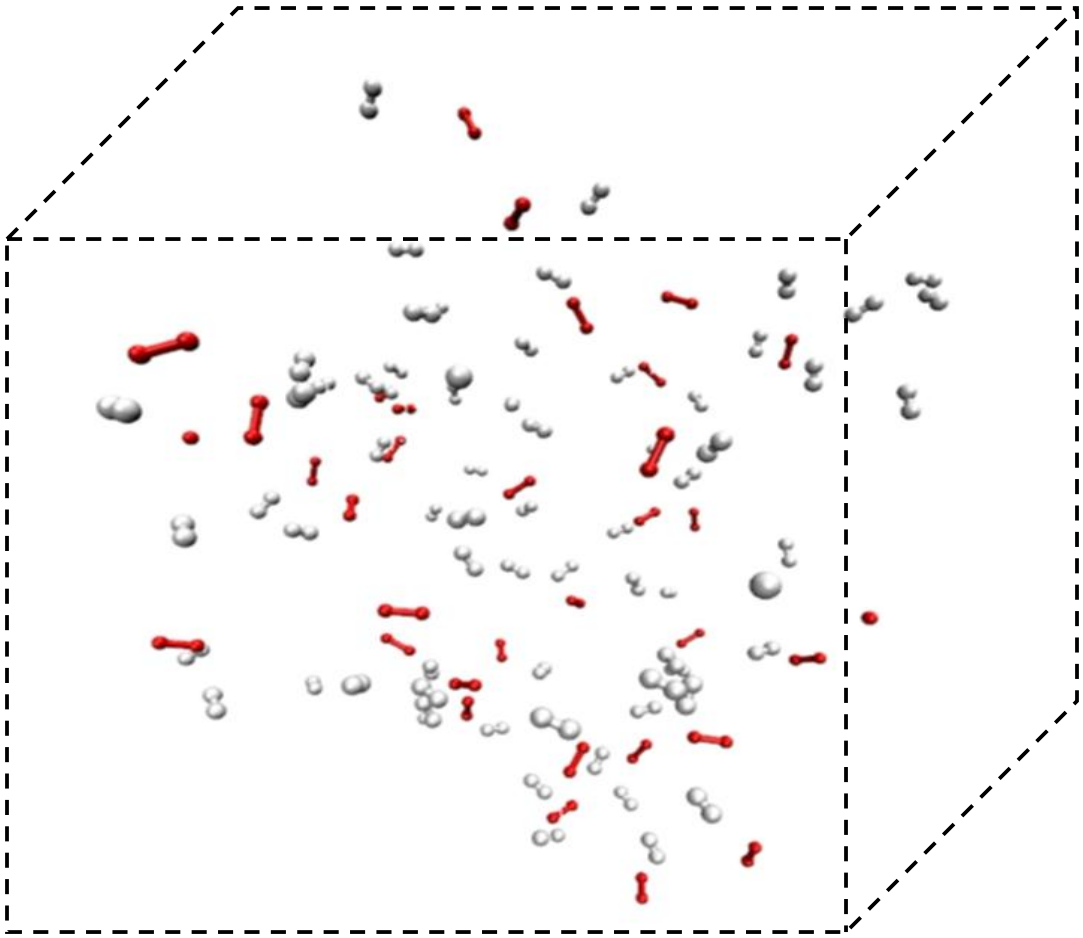

Figure **4-1**: A cubic periodic box of side length 25Å containing 67 H_2 and 33 O_2 molecules (density =0.13kg/dm^3). The red atoms portray O atoms and white atoms represent H atoms. This is the snapshot taken at the beginning of an NVT simulation performed at 3500K.

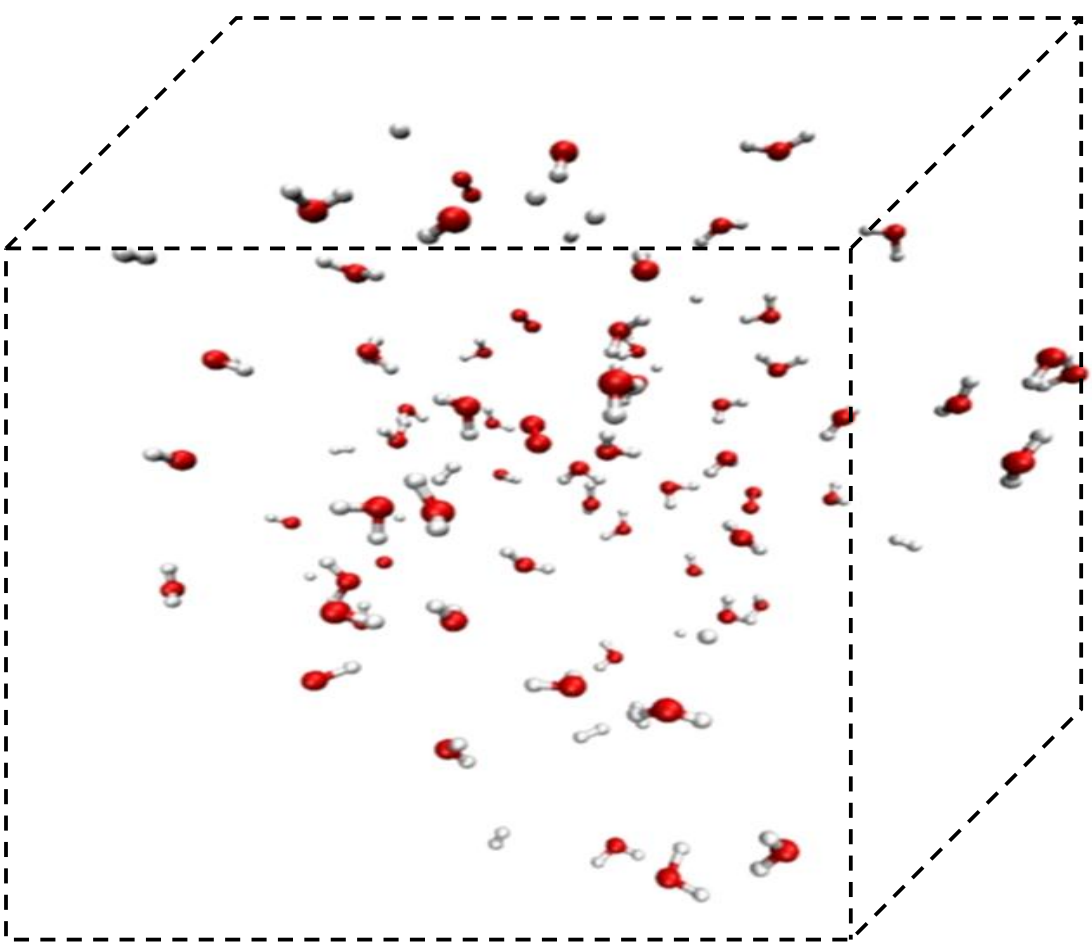

Figure **4-2**: The content of the periodic box changed to 57 H_2O,9 H_2,4 O_2,1 OH and 1 H from 67 H_2 and 33 O_2 after 0.5ns of simulation. This is the snapshot taken at the end of the NVT simulation performed at 3500K. The red atoms portray O atoms and white atoms represent H atoms.

Once the trajectory is obtained, analysis scripts are run to analyze the trajectory for the reaction products, reaction pathway and thermodynamic properties. Since the MD method essentially outputs the position and velocity at each time step using the Newton's equation, trajectory analysis scripts are essential for MD results analysis. The complexity of this analysis drastically increases if we increase the size of system or the time of simulation, because of the drastic increase in size of the trajectory file produced by MD. The ReaxFF MD code already has in-built scripts to obtain the composition of the mixture at each time step. ReaxFF creates a connection table for each atom at each time step using a bond-order cutoff of 0.3Å, to determine

the connectivity of each atom. This bond-order cutoff does not affect the simulations but only the interpretation in terms of chemical components. However for this research we were required to know the reactions occurring at each time step. In order to determine that, we wrote a script which essentially reads the connection table created by ReaxFF and determines the reactions occurring at each time step. The pseudo code for this script can be found in Appendix B.

4.2 Trajectory Analysis Results

Before analyzing the trajectory results, first let us gain perspective of our input conditions (Table 4-1) of the simulations. As explained in section 2.1 of chapter 2 , the hydrogen combustion kinetics is divided into pressure-temperature boundaries of explosion limits(see figure 2-1). Since we are dealing with very high pressure and high temperature, we have an explosive system but the reaction kinetics of the system will be determined by the extended second explosion limit. Using equation 2.1 and rate constant values from Li et al[9], we determined the locus of extended second explosion limit. Assuming [M] to be the total concentration of our system, since the whole system is involved in collisions for the reaction R10 and using ideal gas equation we calculated the pressure as a function of temperature. Hence the modified eq(2.1) becomes

$$\frac{2k_7(T)}{k_{10}(T)} = [M] = \frac{P}{R_u T} \tag{4.1}$$

where T is the temperature, P is the pressure and R_u is the universal gas constant and the rate constants are shown as functions of T. Figure 4-3 shows the extended second explosion limit calculated from equation (4.1). The separate plots of H_2 , O_2 and H_2O imply particular cases, when H_2 , O_2 and H_2O are separately involved in all the third body collisions in R10.

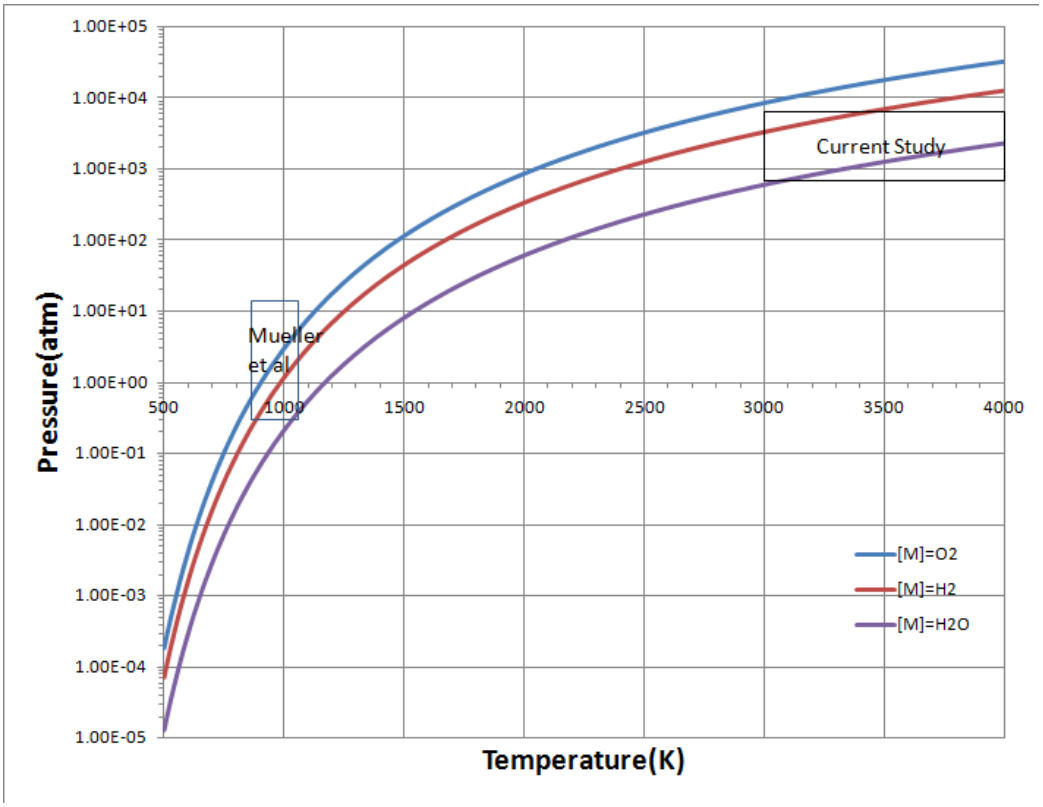

Figure **4-3**: Figure shows the extended second explosion limit calculates using equation 4.1, assuming third body(M) collisions only from H_2,O_2 and H_2O respectively. The collision efficiency values were taken from Li et al[9].

Figure 4-3 suggests that our data lies very close to the extended second explosion limit; as such we could be seeing a transition of reaction kinetics. However, this analysis (equation 4.1) is an approximation since it assumes ideal gas law to hold true at our input conditions. The figure also shows the simulation input conditions for Mueller et al[8] who have analyzed reaction kinetics above the second explosion limit in their manuscript.

4.2.1 Reactivity of H_2/O_2 mixture

For our input conditions (Table 4-1) and simulation time(i.e. 0.5 ns) ReaxFF predicts H_2/O_2 mixtures to be reactive and we observe water formation in our MD simulations, as shown

in figure 4-2. In order to explore further the reactivity of a H_2/O_2 mixture, we have compiled the water formation in a H_2/O_2 mixture as a function of temperature, volume and composition of the system.

4.2.1.1 Water Formation as function of Temperature:

NVT MD simulations were run for a H_2/O_2 mixture (Number of atoms (N=200 ($67H_2$,$33O_2$)) in a cubic periodic box of volume(V =25Åx25Åx25Å), with temperatures (T=3000K,3250K,3500K,3750K and 4000K).Figure 4-4 shows the number of water molecules formed as a function of simulation time for NVT MD run at 3000K. From the trend of curve in figure 4-4 we can observe that reactions in the mixture do not occur continuously. Rather, reaction intiation in the mixture is a rare event and occurs in spurts at locations where initiation reaction occurs. This is obvious, because we are simulating a minuscule system and can expect initiation to occur only in some parts of the system at a time. In order to get the macroscopic behavior of water formation, an average of multiple independent simulations needs to be taken. Hence, for each temperature we performed 5 independent simulations with different initial configurations and calculated the number of water molecules formed after each time step. An average of the number of water molecules formed was calculated from the 5 independent simulations and was plotted as shown in figure 4-5. We observe that water formation is more continuous and the general trends of earlier initiation and faster kinetics with increasing temperature. However, we observe some overlap for the temperatures 3500K and 3750K, which is due to the small system we are simulating and the average being taken over only 5 simulations.

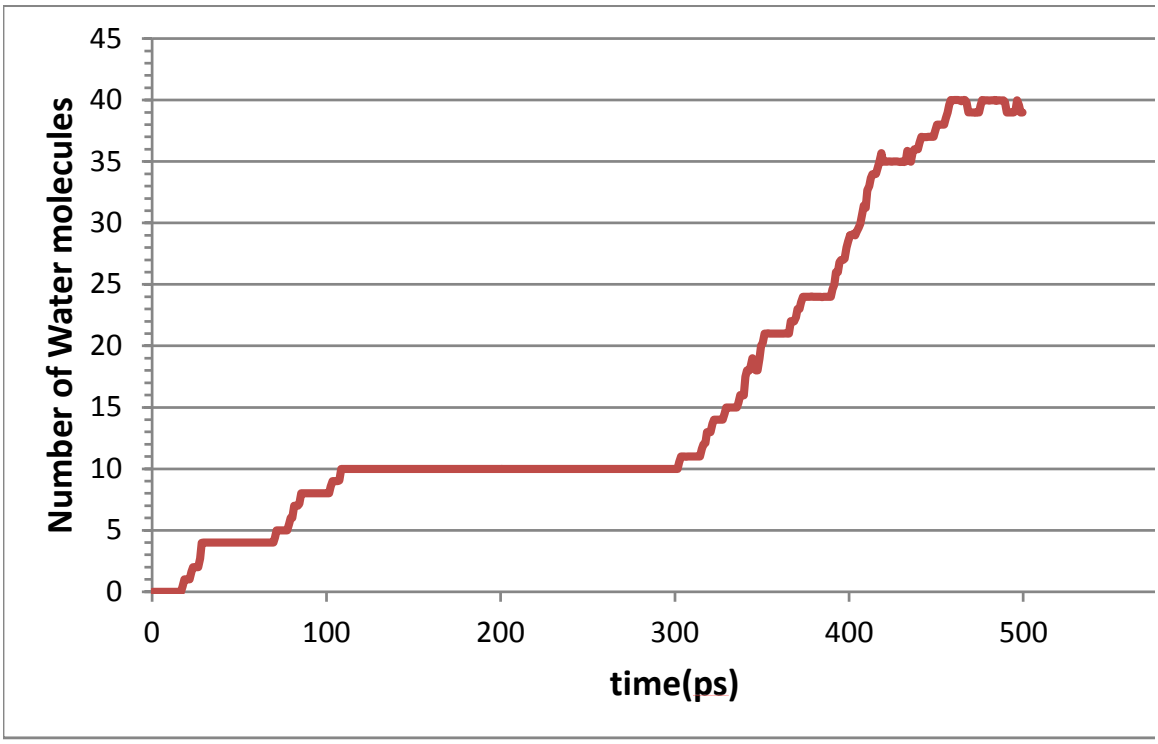

Figure **4-4**: Number of Water molecules formed as a function of time for a NVT simulation run for 0.5ns at 3000K, with $67H_2$,$33O_2$ molecules in a cubic periodic box of side length 25Å

4.2.1.2 Water Formation as function of Volume:

A similar study was done by varying the volume of the cubic periodic box from 20Åx20Åx20Å to 40Åx40Åx40Å, keeping the temperature (T=3500K) and mixture composition (N=200($67H_2$,$33O_2$)) fixed. Figure 4-6 shows water formation against simulation time for 0.5ns of simulation. We observe that in general, the smaller the volume, the earlier is the reaction initiation and the faster is the kinetics.

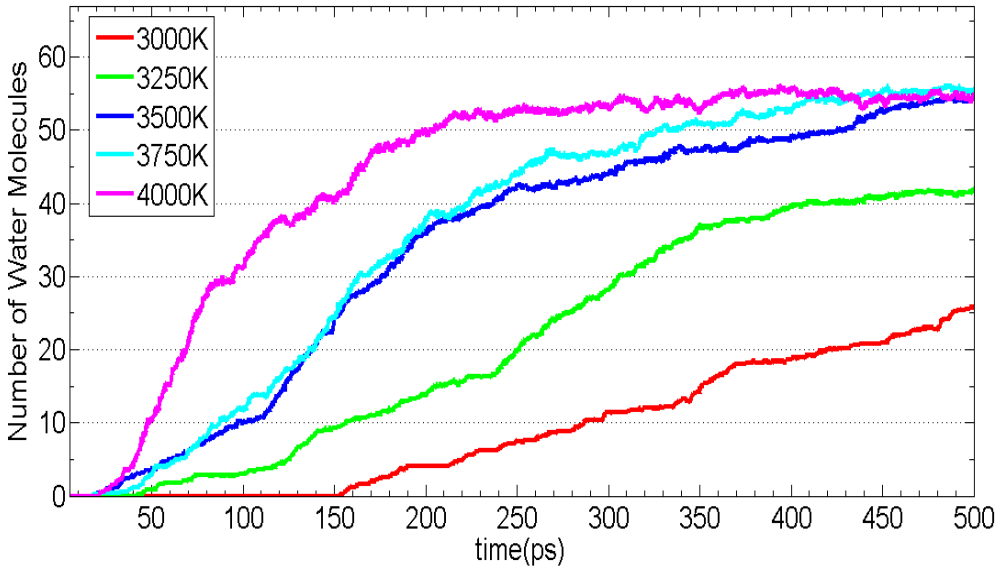

Figure **4-5**: Water formation vs time for varying Temperature. Volume and mixture composition are fixed. The results were obtained from 5 independent simulations at each Temperature.

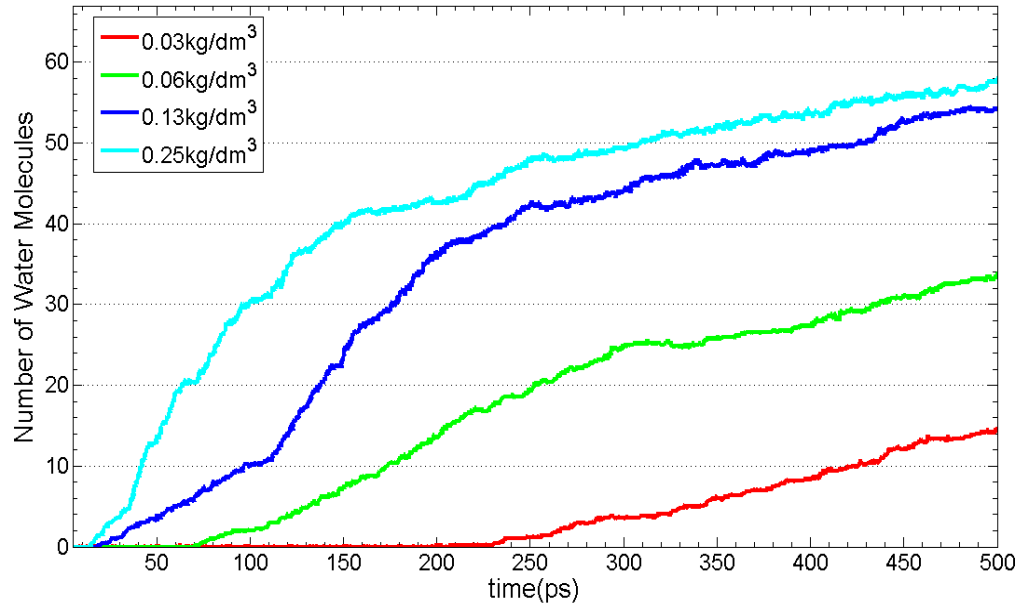

Figure **4-6**: Water formation vs time for varying Volume of periodic box. Temperature and mixture composition are kept fixed. The results were obtained from 5 independent simulations at each Volume.

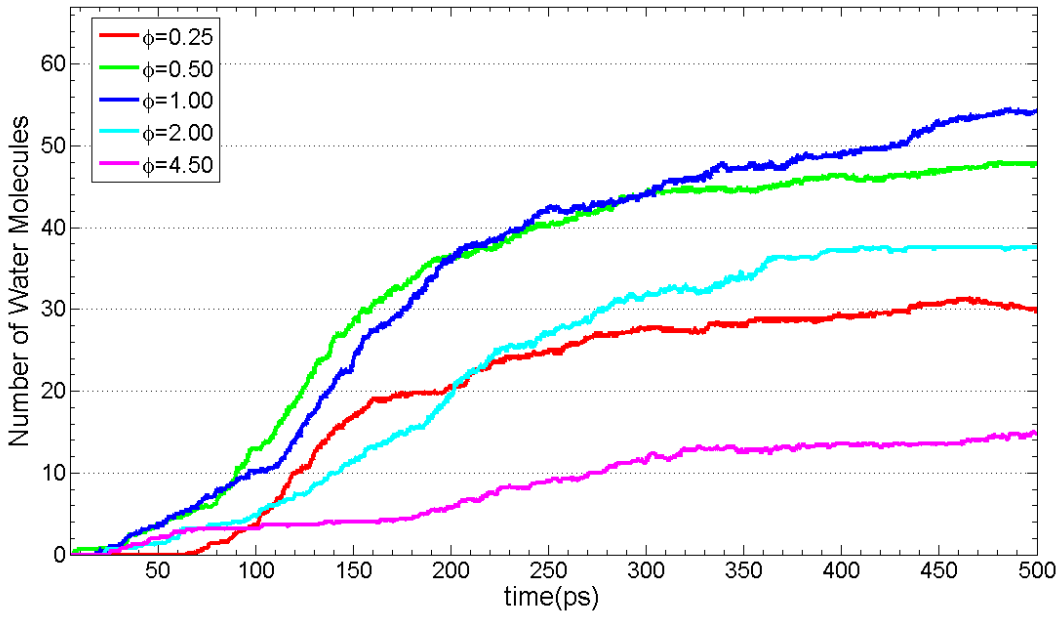

Figure **4-7**: Water formation vs time for varying equivalence ratio. Temperature, Volume of periodic box and number of atoms are kept fixed. The results were obtained from 5 independent simulations at each equivalence ratio.

4.2.1.2 Water Formation as function of Mixture Composition:

The same study is repeated by keeping the Temperature(T=3500K) ,volume(V =25Åx25Åx25Å) and number of atoms (N=200) fixed but varying the equivalence ratio(Φ) of the mixture from 0.25-4.50 .Figure 4-7 shows the water formation against simulation time for 0.5ns of simulation. We observe in general that, stoichimetric mixture(Φ=1) has the fastest reaction kinetics. However, we also observe that the reaction kinetics at lower equivalence ratios(Φ<1) are faster(higher slope) than the reaction kinetics at higher equivalence ratios(Φ>1), until they start falling short of fuel(H_2) and water formation stalls. For example we can see from figure 4-7 that the rate of water formation in the case of Φ=0.5 is much higher than for Φ=2 throughout the simulation time.

4.2.2 Reaction Mechanism Analysis

4.2.2.1 Initiation Reaction:

We have run NVT MD simulations for input conditions as given in Table 4-1. For all these input conditions we observed that the initiation reaction is predominantly

$H_2+O_2 +M(H_2/O_2) \rightarrow H + HO_2+M$ (R22)

where M is a third body which could be H_2 or O_2 in this case, and does not participate in the reaction. According to Westbrook[68] R22 is a probable initiation step which accurately reproduces experimental ignition delay measurements in shock tube and detonation conditions for continuum kinetic models. However at very high temperature($T \geq 3750K$) and low density conditions($0.03kg/dm^3$) we sometimes observe the initiation reaction as

$H_2 + M(H_2/O_2) \rightarrow H + H + M$ (R23)

We investigated the trajectory of the H_2 molecule involved in the initiation reaction R22 in one of our NVT simulations run at 3500K for $67H_2$,$33O_2$ molecules in a 25Åx25Åx25Å periodic box. We observed that the H_2 molecule experiences several collisions with other molecules in the mixture, resulting in vigorous vibrations and rotations before it finally reacts with one O_2 molecule. The process is shown illustratively in Figure 4-8. This behavior is observed at all our input conditions; however each collision does not necessarily lead to reaction, as some vibrationally excited H_2 molecules manage to release their energy by non-reactive collisions.

4.2.2.2 Intermediate Reactions:

The reaction pathway observed at all our simulation conditions (Table 4-1) have predominantly consisted of reactions involving HO_2 and H_2O_2.This is expected due to the high

pressure conditions at which we have performed simulations. Mueller et al[8] suggested that this would be the case when pressure, temperature co-ordinate will lie above the extended second

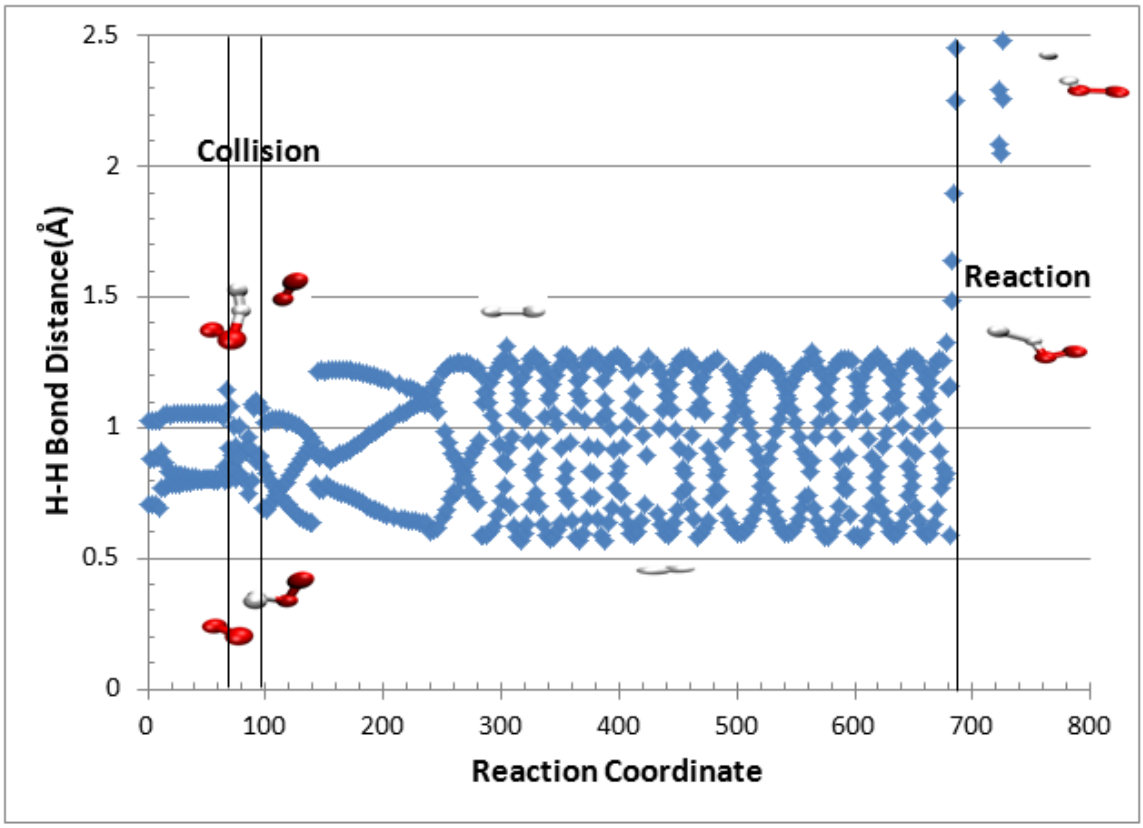

Figure **4-8**: Figure shows the H-H bond distance for the H_2 molecule in reaction R21 ,just before the reaction occurs. We can observe collision of the H_2 molecule with third bodies(M= O_2 in this case) resulting in increase of bond distance due to increased vibrations of the H atoms.

explosion limit. However, the percentage of chain branching reactions R1 and R2 increases when we increase the temperature or increase the volume of periodic box. This gives us a possibility of determining the trend of the extended second explosion limit at high pressure and high temperatures, by simulating at conditions where we see a drift in reaction kinetics.

The reaction intermediates observed in our MD simulations at all input conditions are primarily H, OH, HO_2, O and H_2O_2 molecules before leading to water as the final product. After

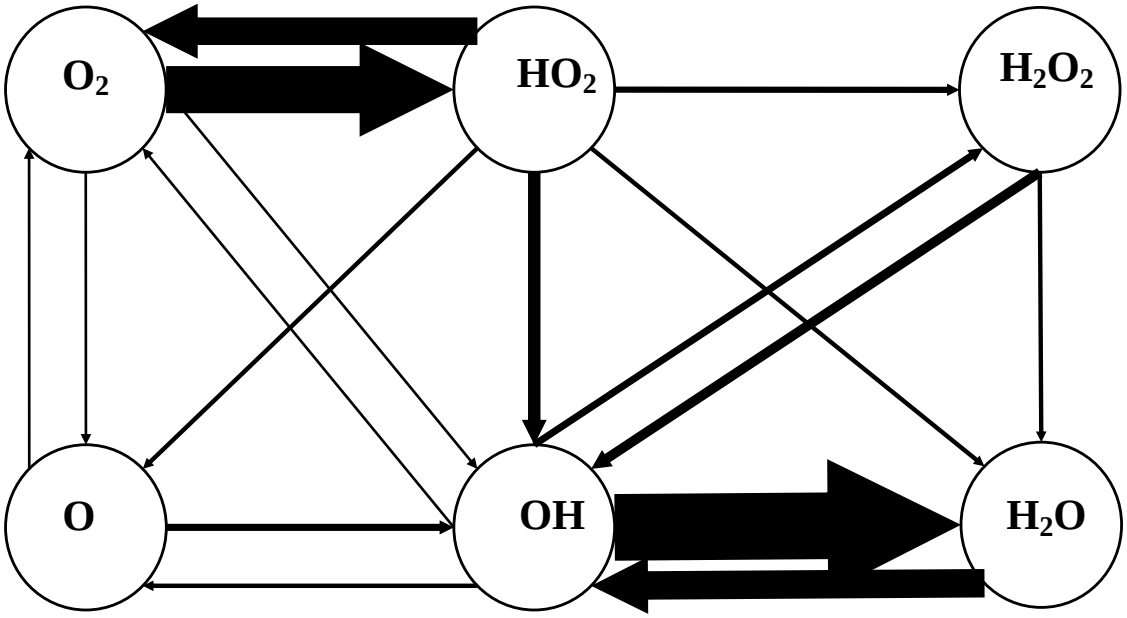

O_2		**H_2O_2**	
$H + O_2 \rightarrow HO_2$	88.6%	$H_2O_2 \rightarrow OH + OH$	54.5%
$H_2 + O_2 \rightarrow H + HO_2$	3.8%	$H_2O_2 + H \rightarrow H_2O + OH$	45.5%
$H_2 + 2O_2 \rightarrow 2HO_2$	3.8%		
$H + O_2 \rightarrow OH + O$	1.9%	**OH**	
$H_2 + O_2 \rightarrow OH + OH$	1.9%	$H_2 + OH \rightarrow H_2O + H$	83.4%
		$H + OH \rightarrow H_2O$	5.1%
HO_2		$OH + OH \rightarrow H_2O_2$	5.1%
$HO_2 \rightarrow H + O_2$	48.1%	$OH + OH \rightarrow H_2O + O$	2.5%
$H + HO_2 \rightarrow OH + OH$	20.4%	$OH + HO_2 \rightarrow H_2O + O_2$	1.3%
$H_2 + HO_2 \rightarrow H_2O_2 + H$	11.1%	$H + OH + O \rightarrow H_2 + O_2$	1.3%
$H + HO_2 \rightarrow H_2 + O_2$	5.5%	$H + OH \rightarrow H_2 + O$	1.3%
$H + HO_2 \rightarrow H_2O + O$	5.5%		
$HO_2 \rightarrow OH + O$	3.7%	**H_2O**	
$H_2 + HO_2 \rightarrow H_2O + OH$	1.9%	$H + H_2O \rightarrow H_2 + OH$	93.8%
$HO_2 + OH \rightarrow H_2O + O_2$	1.9%	$H_2O \rightarrow H + OH$	3.1%
$HO_2 + H_2O \rightarrow H_2O_2 + O_2$	1.9%	$H_2O + O \rightarrow OH + OH$	3.1%
O			
$H_2 + O \rightarrow H + OH$	77.8%		
$H_2O + O \rightarrow OH + OH$	11.1%		
$H + OH + O \rightarrow H_2 + O_2$	11.1%		

Figure **4-9**: Figure shows the O_2 reaction pathway, for the input conditions (3500K, 25Åx25Åx25Å, ($67H_2$,$33O_2$)), over a simulation time of 0.5ns. The thickness of the arrows is proportional to the number of molecules consumed of the species at the rear end of the arrow to form the front end species (normalized by OH $\rightarrow H_2O$ case). The table below lists the reactions involved in the paths shown along with their percent contribution to the destruction of a given species.

the initiation reaction, the reaction pathway primarily consists of consumption of H radicals by O_2 molecules in the mixture to form HO_2 radicals. The HO_2 radicals then react to get converted to OH radicals. Finally, the OH radicals consume H_2 molecules to form water and H radicals which continue the chain of reactions. The reaction pathway is shown illustratively for one of the NVT simulations in figure 4-9. Mueller et al[8] predicted a similar reaction pathway for input conditions lying above the extended second explosion limit.

4.2.2.3 Overall Activation Energy:

The overall water formation reaction from H_2/O_2 is simply

$H_2 + 1/2O_2 \rightarrow H_2O$ (R24)

In order to calculate the overall activation energy of this reaction, we performed NVT MD simulations of pure H_2/O_2 mixtures (N=200(Φ =1), V =25Åx25Åx25Å & V =32Åx32Åx32Å) for temperatures ranging from 3000K-4000K. For each temperature, 5 simulations with different initial configurations were run. The average rate constant of the overall reaction is evaluated as

$$k_{ov} = -\frac{d[H_2]}{dt}\frac{1}{[H_2]\sqrt{[O_2]}} \quad (4.2)$$

where $[H_2]$,$[O_2]$ is the average concentration of H_2,O_2 from the 5 independent simulations respectively. $\frac{d[H_2]}{dt}$ is calculated by fitting a curve to the average $[H_2]$ concentration profile and evaluating its slope. The activation energy is evaluated using the Arrhenius rate equation i.e.

$$k_{ov} = A\exp(-E_a/RT) \quad (4.3)$$

We obtained activation energy values of 34.26±3.28 kcal/mole for V =25Åx25Åx25Å and 55.73±4.97 kcal/mole for V =32Åx32Åx32Å. While both these values are much greater than the overall activation energy of 16kcal/mole in the chain explosive regime, we had no existing experimental/continuum model data at our input conditions to compare our results with. Mueller

at al[8] conducted a similar study and found the overall activation energy to be 61±10 kcal/mol for lean $H_2/O_2/N_2$ mixtures(P=6.5 atm, T=884-934K, Φ =0.3). While their input conditions lie above the extended second explosion limits, they are certainly different from our case. They have conducted constant pressure simulations, while on the other hand we have conducted simulations at constant temperature.

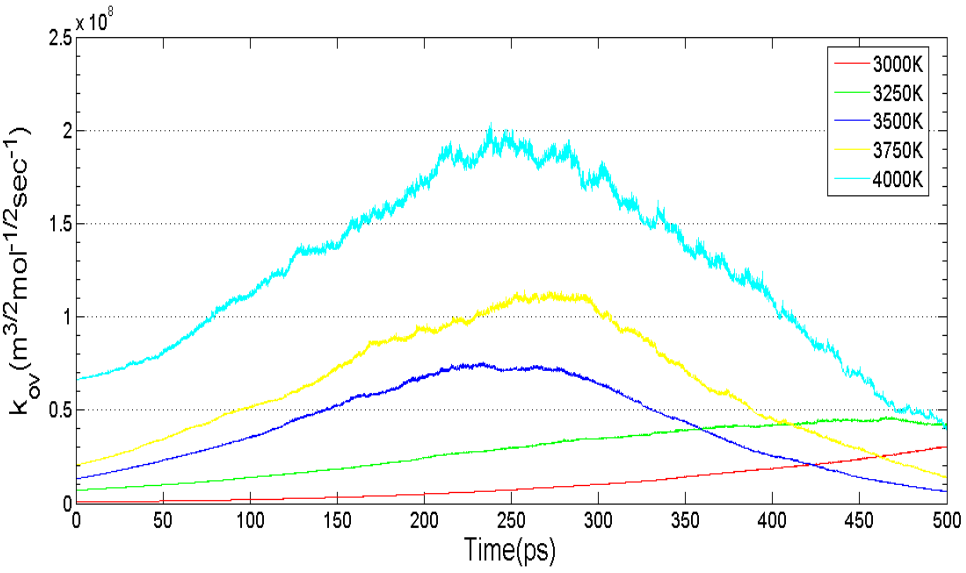

Figure **4-10**: The average overall rate constant calculated at every time step for NVT MD simulations run for $67H_2$,$33O_2$ molecules for V=32Åx32Åx32Å and temperature from 3000K-4000K.

The average overall rate constants calculated as a function of time in our analysis show an interesting trend as shown in figure 4-10. We can observe that, the overall rate constant of the reaction increases from a low value to a certain peak and then goes down. This suggests that, the rate of reaction is slow during initiation, and it peaks during the intermediate reactions stage, where water formation occurs rapidly and gradually decreases as the fuel (H_2) gets consumed. At higher temperatures we reach the reaction constant maximum earlier.

In our derivation for activation energy(refer equation 4.3), we have taken k_{ov} to be the average of the rate constant over the whole simulation time for each temperature. This may not be a correct assumption, because at the various temperatures we are simulating the reaction regimes are different. While at lower temperatures(for 3000K and 3250K in figure 4-10), most of the simulation data lies in the initiation regime and the peak in reaction comes very late, while at higher temperatures(3750K and 4000K in figure 4-10) the reactions are complete within the simulation time. This is a problem because our input conditions as figure 4-3 suggests could be lying in the transition phase of the extended second explosion limit. One way of evaluating the correct activation energy would be to consider similar reaction regimes for each temperature. This will be a part of our future work in this research.

4.2.2.4 Mixture seeded with one OH radical

We performed NVE MD(microcanonical ensemble) simulations for H_2/O_2 mixtures seeded with 1OH radical (67 H_2,32 O_2, 1OH molecule in a 20Åx20Åx20Å periodic box) as a test to observe transition of reaction kinetics. Starting with a temperature of 2000K, we performed the simulations for a period of 0.5ns. We observed that water formation occurs very early in the simulation due to presence of OH radical in the mixture, by the following reaction:

$H_2 + OH \rightarrow H_2O + H$ (R25)

This is followed by

$H + O_2 \rightarrow HO_2$ (R26)

We also observe that reaction occurs very slowly till around 200-250ps, after which there is a sudden rise in reaction rate as well as the Temperature of the mixture, suggesting a transition of reaction conditions from thermal/chain explosive region(slow kinetics) to chain branching explosive region(fast kinetics)(see figure 4-11). This type of analysis will be useful to determine

the location of second explosion limits for high temperature and high pressure conditions, and will be explored in our future research work.

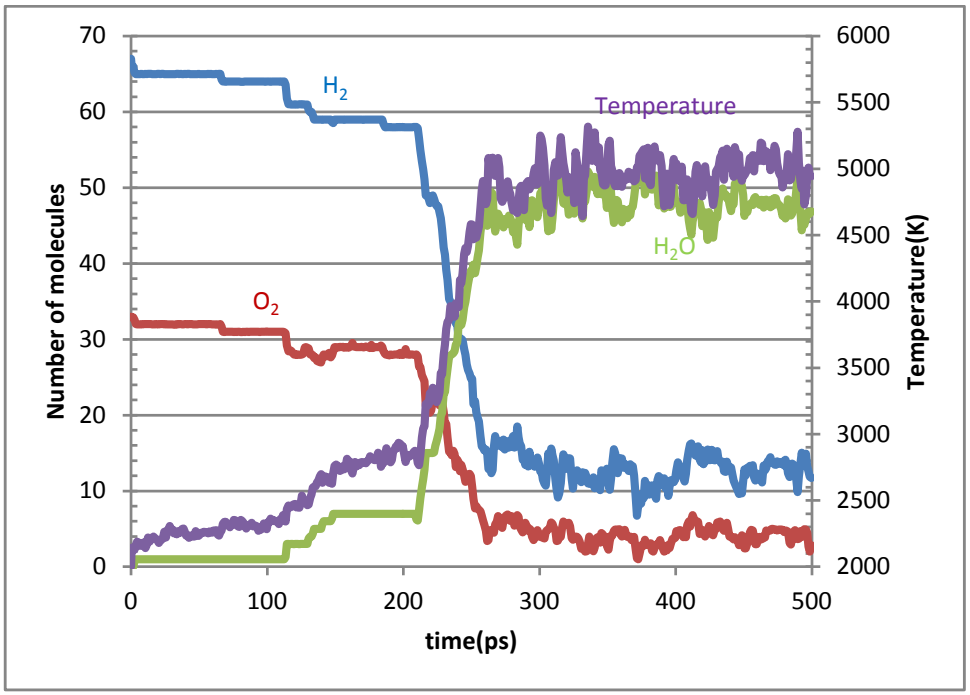

Figure **4-11**: Water formation vs. time for NVE MD simulation of hydrogen/oxygen mixture(67 H_2 and 32 O_2 molecules) seeded with 1OH radical with initial temperature(T = 2000K) and volume(20Åx20Åx20Å).The figure also shows consumption rate of H_2 and O_2 and temperature profile.

Chapter 5

CONCLUSION

We have described an application of ReaxFF for getting a more detailed understanding of the reaction kinetics of hydrogen combustion. The ReaxFF force field was parameterized against experimental data containing reaction energy and transition state data of important reactions of hydrogen combustion. Quantum mechanics derived bond energy, valence angle energy, torsion angle energy, bond formation/dissociation profiles and heat of formations were also added to the training set. The optimized force field was used to perform a range of NVT Molecular Dynamics simulation(i.e. Molecular Dynamics simulation with constant number of atoms, volume and temperature) to elucidate the reaction kinetics of hydrogen combustion at our input conditions.

Under all our input conditions ($2750K \leq T \leq 4000K$, $0.25 \leq \Phi \leq 4.5$, $0.03 kg/dm^3 \leq density \leq 0.25 kg/dm^3$), the initiation reaction was found to be predominantly reaction R22 i.e.

$$H_2 + O_2 + M(H_2/O_2) \rightarrow H + HO_2 + M \qquad (R22)$$

The rate of water formation for a fixed density and fixed equivalence ratio was found to increase with temperature. Similarly for fixed temperature and equivalence ratio, rate of water formation increased with increase in mixture density. The rate of water formation was found to be maximum for a stoichiometric mixture of hydrogen and oxygen, at a fixed temperature and fixed density. The rate of water formation decreased for both fuel lean and fuel rich mixtures, with fuel rich mixtures having a lower rate of formation. Reaction initiation was found to be faster for higher temperature and higher densities.

The intermediate reactions in the NVT MD simulations were found to be dominantly consisting of formation and consumption reactions of HO_2 and H_2O_2. Most of the oxidizer O_2 gets converted into the hydroperoxyl radical instead of choosing the chain branching reaction pathway i.e.

$H + O_2 \rightarrow OH + O$ (R1)

$H_2 + O \rightarrow OH + H$ (R2)

$H_2 + OH \rightarrow H_2O + H$ (R3)

However, a shift in kinetics from HO_2/H_2O_2 pathway to chain branching reactions R1 and R2 was observed with increasing temperature and decreasing density. The overall activation energy of hydrogen combustion found was much higher than 16 kcal/mol, which suggests that our input conditions do not lie in the chain explosive region. However we need to calculate activation energies over the same reaction regimes for different temperatures, in order to understand better, the reaction kinetics occurring in those regimes.

From these results, we can say that ReaxFF can be a useful tool to elucidate complex reaction mechanisms and obtaining reaction kinetic data. With our newly added reaction mechanism analysis tool, it is possible to study in greater detail the initiation and intermediate reactions. ReaxFF can be used to simulate reactions at a variety of input conditions, which are otherwise difficult to perform experimentally and its results can be used to improve existing continuum-scale kinetic models.

5.1 Future Work

As of now we are working on two projects related to hydrogen combustion. One of them is conducting large scale simulations of hydrogen combustion i.e. $o(10^4)$ atoms. The aim of this project is to capture explosive behavior of a H_2/O_2 mixture and analyze the shock waves created around a reaction zone.

Another project is to develop a ReaxFFforce field for accurately simulating catalytic effects of a Platinum surface in presence of a H_2/O_2 mixture. This is important from the

perspective of flow-reactor experiments, where ignition delay measurements are affected due to catalytic reactions on the reactor walls[69].

BIBLIOGRAPHY

1. Marban, G; Valdes-Solis, T. Int J Hydrogen Energy 2007, 32, 1625–37.
2. Midilli, A; Dincer, I. Int J Hydrogen Energy 2008, 33, 4209–22.
3. Schlapbach, L.; Zuttel, A. Nature 2001, 414, 353-358.
4. Palumbo, O.; Paolone, A.; Rispoli, P.; Cantelli, R. Materials Science and Engineering a-Structural materials 2009, 521-522, 134-138.
5. Petukhov, V.A.; Naboko, I.M.; Fortov, V.E. International Journal of Hydrogen Energy 2009, 34, 5924-5931.
6. von Elbe, G.; Lewis, B. Combustion, Flames, and Explosions of Gases, 3rd ed; Academic: Orlando, FL, 1987.
7. Dixon-Lewis, G.; Williams, D. J. In Comprehensive Chemical Kinetics; Bamford, C. H.; Tipper, C.F.H.,Eds.; Elsevier Scientific: Amsterdam, 1977.
8. Mueller, MA; Kim, TJ; Yetter, RA; Dryer, FL International Journal of Chemical Kinetics 1999, 31, 113-125.
9. Li, J.; Zhao, Z.; Kazakov, A.; Dryer, F. International Journal of Chemical Kinetics 2004, 36, 566-575.
10. Strohle, J.; Myhrvold, T. International Journal of Hydrogen Energy 2007, 32, 125-135.
11. Ó Conaire, M.; Curran, H; Simmie, J; Pitz, W; Westbrook, C. International Journal of Chemical Kinetics 2004, 36, 603-622
12. Raty, J.; Gygi, F.; Galli, G. Phys. Rev. Lett. 2005, 95, 096103
13. Case, D.A.; Darden, T.A.; Cheatham, T.E., III; Simmerling, C.L.; Wang, J.; Duke, R.E.; Luo, R.; Walker, R.C.; Zhang, W.; Merz, K.M.; Roberts, B.P.; Wang, B.; Hayik, S.; Roitberg, A.; Seabra, G.; KolossvÃ¡ry, I.; Wong, K.F.; Paesani, F.;

Vanicek, J.; Wu, X.; Brozell, S.R.; Steinbrecher, T.; Gohlke, H.; Cai, Q.; Ye, X.; Wang, J.; Hsieh, M.-J.; Cui, G.; Roe, D.R.; Mathews, D.H.; Seetin, M.G.; Sagui, C.; Babin, V.; Luchko, T.; Gusarov, S.; Kovalenko, A.; Kollman, P.A. 2010, AMBER 11, University of California, San Francisco.

14. Cygan, R. T.; Liang, J.-J.; Kalinichev, A. G. J. Phys. Chem. B 2004, 108, 1255-1266
15. Rappe, A. K.; Casewit, C. J.; Colwell, K. S.; Goddard, W. A., III; Skiff, W. M. J . Am. Chem. Soc.1992, 114, 10024-10035.
16. Mayo, S.L.; Olafson, B.D.; Goddard, W., III J . Phys. Chem. 1990, 94, 8897-8909
17. Lii, J.; Allinger, N.L. J . Am. Chem. Soc.1989, 111 , 8576-8582
18. Stuart, S.J.; Tutein, A.B.; Harrison, J.A. J. Chem. Phys. 2000, 112, 6472-6486
19. Brenner, D.W. Phys. Rev. B 1990, 42, 9458-9471
20. Polzer, T.; Kiefer W. Journal of Organometalic Chemistry 1996, 508, 153-157
21. Tersoff, J. Phys. Rev. B 1988, 37, 6991
22. van Duin, A. C. T.; Dasgupta, S.; Lorant, F.; Goddard, W. A., III. J. Phys. Chem. A 2001, 105, 9396.
23. R.A. Yetter, F.L. Dryer, D.M Golden, in: M.Y. Hussaini, A. Kumar, F.G. Voigt (Eds.), Major Research Topics in Combustion, Springer-Verlag, New York, 1992, p. 309-315
24. Glassman, I.; Yetter, R.A. Combustion , 4th ed; Academic Press: San Diego, CA, 2008.
25. Alder, B.J.; Wainwright, T.E. Phys. Rev. 1962, 127, 359–361.
26. Lee, M.R.; Tsai, J.; Baker, D.; Kollman, P.A. J Mol Biol. 2001, 313, 417-430.
27. Fichthorn , K.A.; Miron, R.A.; Wang, Y.; Tiwary, Y. J. Phys.: Condens. Matter 2009, 21, 084212 .

28. Laurendeau, N.M. Statistical Thermodynamics, 1st ed; Cambridge University Press: New York, 2005.
29. Berendsen, H. J. C.; Postma, J. P. M.; van Gunsteren, W. F.; DiNola,A.; Haak, J. R. J. Chem. Phys. B 1984, 81, 3684.
30. Andersen, H.C.; J. Chem. Phy. 1980, 72, 2384
31. Nose, S. Mol. Phy. 1984, 52, 255
32. Hoover, W.G. Phys. Rev. A 1985, 31, 1695
33. Hoover, W.G. Phys. Rev. A 1986, 34, 2499
34. Parinello, M.; Rahman, A. J. Appl. Phys 1981, 52, 7182
35. Frenkel, D.; Smit B. Understanding Molecular Simulation, 2nd ed; Academic Press: San Diego, CA, 2002.
36. Verlet, L. Physical Review volume 1967,159, 98.
37. Swope, W.C.; Andersen, H.C.; Berens, P.H.; Wilson, K.R. J. Chem. Phys. 1982, 76, 637.
38. Born, M.; Oppenheimer, J.R. Ann. Physik 1927, 84, 457
39. B. R. Brooks, C. L. Brooks III, A. D. Mackerell, L. Nilsson, R. J. Petrella, B. Roux, Y. Won, G. Archontis, C. Bartels, S. Boresch A. Caflisch, L. Caves, Q. Cui, A. R. Dinner, M. Feig, S. Fischer, J. Gao, M. Hodoscek, W. Im, K. Kuczera, T. Lazaridis, J. Ma, V. Ovchinnikov, E. Paci, R. W. Pastor, C. B. Post, J. Z. Pu, M. Schaefer, B. Tidor, R. M. Venable, H. L. Woodcock, X. Wu, W. Yang, D. M. York, and M. Karplus J. Comp. Chem. 2009, 30, 1545-1615.
40. Strachan, A.; van Duin, A. C. T.; Chakraborty, D.; Dasgupta, S.;Goddard, W. A., III. Phys. Rev. Lett. 2003, 91, 098301.
41. Strachan, A.; Kober, E. M.; van Duin, A. C. T.; Oxgaard, J.;Goddard, W. A., III. J. Chem. Phys. 2005, 122, 054502.

42. van Duin, A. C. T.; Zeiri, Y.; Dubnikova, F.; Kosloff, R.; Goddard,W. A., III. J. Am. Chem. Soc. 2005, 127, 11053.

43. Chenoweth, K.; Cheung, S.; van Duin, A. C. T.; Goddard, W. A.,III; Kober, E. M. J. Am. Chem. Soc. 2005, 127, 7192.

44. Goddard, W. A., III; van Duin, A.; Chenoweth, K.; Cheng, M. J.;Pudar, S.; Oxgaard, J.; Merinov, B.; Jang, Y. H.; Persson, P. Top. Catal. 2006, 38, 93.

45. Goddard, W. A., III; Merinov, B.; van Duin, A.; Jacob, T.; Blanco,M.; Molinero, V.; Jang, S. S.; Jang, Y. H. Mol. Simul. 2006, 32 251.

46. Buehler, M. J.; van Duin, A. C. T.; Goddard, W. A., III. Phys.Rev. Lett 2006, 96, 095505.

47. Ludwig, J.; Vlachos, D. G.; van Duin, A. C. T.; Goddard, W. A.,III. J. Phys. Chem. B 2006, 110, 4274.

48. Cheung, S.; Deng, W. Q.; van Duin, A. C. T.; Goddard, W. A.,III. J. Phys. Chem. A 2006, 109, 851.

49. Nielson, K. D.; van Duin, A. C. T.; Oxgaard, J.; Deng, W. Q.;Goddard, W. A., III. J. Phys. Chem. A 2005, 109, 493.

50. Zhang, Q.; Cagin, T.; van Duin, A.; Goddard, W. A., III; Qi, Y.; Hector, L. G. Phys. Rev. B 2004, 69, 045423.

51. Chenoweth, K.; vanDuin, A.; Goddard, W.A., III J. Phys. Chem. A 2008, 112, 1040-1053.

52. Pauling, L. J. Am. Chem. Soc. 1947, 69, 542

53. Mortier, W.J.; Ghosh, S.K.; Shankar, S.J. J. Am. Chem. Soc. 1986, 108, 4315

54. Rappe´, A.K.; Goddard, W.A. J. Phys. Chem. 1991, 95, 3358

55. van Duin, A. C. T.; Baas, J. M. A.; van de Graaf, B. J. Chem.Soc., Faraday Trans. 1994, 90, 2881

56. Jaguar,version 7.5; Schrodinger, LLC, New York, NY, 2008.

57. Becke, A. D. J. Chem. Phys. 1993, 98, 5648.

58. Lee, C.; Yang, W.; Parr, R. G. Phys. Rev. B 1988, 37, 785.

59. Krishnan, R.; Binkley, J. S.; Seeger, R.; Pople, J. A. J. Chem. Phys.1980, 72, 650.

60. Curtiss, L.; Raghavachari, K.; Redfern, P.; Rassolov, V.; Pople, J. J. Chem. Phys. 1998 , 109, 7764.

61. Curtiss, L.; Raghavachari, K.; Redfern, P.; Pople, J. J. Chem. Phys. 2000, 112, 7374

62. Argonne National Laboratory-Chemical Sciences and Engineering. "Energies of G2/97 Test Set: neutrals". Argonne National Laboratory. http://www.cse.anl.gov/OldCHMwebsiteContent/compmat/g3energies/g3neut.htm

63. Argonne National Laboratory-Chemical Sciences and Engineering. "Energies of G2/97 Test Set: ions". Argonne National Laboratory. http://www.cse.anl.gov/OldCHMwebsiteContent/compmat/g3energies/G3aux.htm

64. Leach, A.R. Molecular Modeling, 2nd ed, Pearson Education Limited: Essex, England, 2001.

65. Yetter, R.A.; Rabitz, H.; Hedges, R.M. J Chem Kinetics 1990, 23, 251

66. Baulch, D. L.; Bowman, C. T.; Cobos, C. J.; Cox, R. A.; Just, Th.; Kerr, J. A.; Pilling, M. J.; Stocker, D. ; Troe, J.; Tsang, W.; Walker, R. W. ; Warnatz, J. J. Phys. Chem. Ref. Data 2005,34.

67. Shanno, D.F. Mathematics of Operations Research 1978, 3, 244-256.

68. Westbrook, C.K. Comb Sci Tech 1982, 29, 67.

69. Chaos, M.; Dryer, F.L. Comb Sci Tech 2008, 180, 1053-1096.

APPENDIX A
Optimized ReaxFF parameters for H_2/O_2 mixtures

I have tabulated some of the important parameters, which we optimized by our training set. Following are the parameters listed in this appendix:

1. Parameters relevant to H and O atoms: These parameters primarily correspond to non-bonded interaction potential functions(coulomb, van der Waal, lone pair), and parameters dependent only on the atoms. The parameters comprise of van Der Waal radius, covalent bond radius, electronegativity, electrical hardness, bond-order correction related parameters.(see Table A-1)
2. Parameters relevant to bonds between H and O atoms: These parameters correspond to parameters relevant to pair-wise bonded interaction potential functions. They consist of parameters like equilibrium bond length, bond dissociation energy, force constant etc.(see Table A-2 and A-3)
3. Parameters relevant to valence angles between combinations of H and O atoms: These parameters correspond to three-body potential functions in ReaxFF. They primarily consist of parameters like equilibrium valence angle, force constants etc.(see Table A-4).
4. Parameters relevant to torsion angles between combinations of H and O atoms: These parameters correspond to four-body interaction potential functions in ReaxFF. They primarily consist of parameters like force constants etc.(see Table A-5).
5. Parameters relevant to hydrogen bonding: These consist of parameters relevant to hydrogen bonding potential function in ReaxFF.(see Table A-6).

For more information on the ReaxFF potential functions and parameters used in them, refer to supporting material of Chenoweth et al[51].

Table **A-1**: ReaxFF atom parameters for H and O.

	r_o	$p_{ov/un2}$	Coulomb Parameters		
			η(eV)	χ(eV)	γ($Å^{-1}$)
H	0.7060	-27.3241	7.5	6.2020	1.0000
O	1.4081	-3.5104	7.5	8.5000	1.0000

	p_{lp2}	van der Waals parameters			
		r_{vdw}(Å)	α(alfa)	γ_{vdw}($Å^{-1}$)	ϵ(kcal/mol)
H	0.0000	1.7219	8.1050	33.2894	0.0837
O	0.8435	2.4347	9.8475	13.8449	0.0928

Table **A-2**: ReaxFF van der Waals and bond radius parameters for the H-O bond.

Bond	r^{σ}(Å)	r_{vdw}(Å)	ϵ(kcal/mol)	γ_{vdw}($Å^{-1}$)
H-O	0.9951	1.2594	0.0377	11.6668

Table **A-3**: ReaxFF bond energy and bond-order parameters for H-H, H-O and O-O bonds.

Bond	D^{σ}_e(kcal/mol)	$p_{be,1}$	$p_{be,2}$	$p_{bo,1}$	$p_{bo,2}$	D^{π}_e(kcal/mol)
H-H	157.5488	-0.1661	6.2500	-0.0346	5.8275	0.0000
H-O	216.7852	-1.0000	1.6492	-0.1610	4.0000	0.0000
O-O	122.9794	1.0000	0.1958	-0.1101	7.0000	211.2666

Table **A-4**: ReaxFF valence angle parameters for H-H-H,H- H-O,H-O-H,H-O-O,O-H-O and O-O-O angles.

Valence Angle	$\Theta_{(0,0)}$(deg)	p_{val1}(kcal/mol)	p_{val2}(1/radian^2)	p_{val7}	p_{val4}
H-H-H	0.0000	45.0000	7.5481	0.0500	1.4015
H-H-O	0.0000	10.0000	2.0000	3.0000	1.9962
H-O-H	83.0482	22.0003	1.0000	3.0000	1.0400
H-O-O	77.7270	10.4778	2.3630	3.0000	1.5944
O-H-O	0.0000	25.0000	1.0000	0.5139	1.6785
O-O-O	90.0000	2.5000	1.0000	0.6121	3.0000

Table **A-5**: ReaxFF torsion angle parameters .

Torsion Angle	V_1(kcal/mol)	V_2(kcal/mol)	V_3(kcal/mol)	$p_{tor,1}$	$p_{cot,1}$
H-O-O-H	2.5000	26.0267	1.0000	-7.5890	-1.0000
H-O-O-O	0.8302	-4.0000	-0.7763	-2.5000	-1.0000
O-O-O-O	-2.5000	-4.0000	1.0000	-2.5000	-1.0000

Table **A-6**: ReaxFF hydrogen bond parameters .

Bond	r_{hb}(Å)	$p_{hb,1}$	$p_{hb,2}$	$p_{hb,3}$
O-H-O	2.1200	-3.5800	1.4500	19.5000

APPENDIX B
Algorithm to Extract Reaction from MD Trajectory

As discussed in section 4.1 of chapter-4, we need to extract reactions from the trajectory file of ReaxFF, in order to find out the reaction mechanism. Following is a pseudo code for finding out the reaction, that a certain atom J(say) at a certain time is involved in, from the trajectory file. The target of the pseudo code is to find all the atoms involved in the reaction, using information of the connection table of atoms in the simulation.

1. Let the atom be atomJ, Let the time be I
2. List1 = 0, Size_List1 = 0
3. List2 = 0, Size_List2 = 0
4. List3 = 0, Size_List3 = 0
5. List3= Atoms connected to atom J at time I(including itself) [Connection Table for each atom are available from ReaxFF]

   Size_List3= size of List3,
6. While (Size_List3 != Size_List1)
7. List1 = List3

   Size_List1 = Size_List3

   List2 = Unique list of atoms connected to each atom in List1 at time I+1(i.e. after one time step)

   List3 = Unique list of atoms connected to each atom in List2 at time step I.

   Size_List3 = size of List3
8. End While Loop
9. List1 has the list of all atoms involved in the reaction involving atomJ.

   The molecules comprising atoms in List1 for time I are the reactants

The molecules comprising atoms in List1 for time step I+1 are the products

Following is a snapshot of a subroutine which takes a list of atoms and returns the list of reactions, those atoms are involved in. The code is written using C and has made extensive use of the C++ STL library.

```
void solveReaction(vector<int>& aList,vector<int>&
a2mR,vector<int>& a2mP,multimap<int,int>&
m2aR,multimap<int,int>&m2aP,vector< vector<int> >&
reacMList,vector< vector<int> >& prodMList,list<int>&
molListReac,list<int>& molListProd)
{
  // Solves the reaction for a given Atom List(taken as reactant
side).

  reacMList.clear();
  prodMList.clear();
  vector<int> xAList1,xAList2,xAList3;

  reacMList.push_back(aList);

  xAList1.clear();
  xAList2.clear();
  xAList3.clear();
  xAList3 = aList;

  while(xAList1.size() != xAList3.size())
    {
      xAList1 = xAList3;
      a2mList(xAList1,a2mP,m2aP,prodMList,molListProd,xAList2);

      a2mList(xAList2,a2mR,m2aR,reacMList,molListReac,xAList3);
      xAList2.clear();
    }

  // reacMList contains list of reactants
  // prodMList contains list of products
}


void a2mList(vector<int>& aList,vector<int>& a2m,multimap<int,
int>& m2a,vector<vector<int> >& mList,list<int>&
molNumList,vector<int>& xAList)
{
  mList.clear();
  xAList.clear();
```

```
  //finds list of molecules corresponding to 'aList'
  //finds list of unique atoms in the list of molecules


  // First find molecule numbers of the atoms
  list<int> molnum;
  for(int i = 0 ; i < aList.size() ; i++)
    molnum.push_back(a2m[aList[i]]);
  molnum.sort();
  molnum.unique();

  // Now find the list of atoms corresponding to each molecule
  m2aList(molnum,m2a,mList);
  for( int i = 0 ; i < mList.size(); i++ )
    {
      for(int j = 0 ; j < mList[i].size() ; j++)
     xAList.push_back(mList[i][j]);
    }
  molNumList = molnum;
}
```